JOURNAL OF GEOPHYSICAL RESEARCH, VOL. 114, A01211, doi:10.1029/2008JA013225, 2009

A state-of-the-art picture of substorm-associated evolution of the near-Earth magnetotail obtained from superposed epoch analysis

Y. Miyashita,[1] S. Machida,[2] Y. Kamide,[3] D. Nagata,[2] K. Liou,[4] M. Fujimoto,[1] A. Ieda,[5] M. H. Saito,[1] C. T. Russell,[6] S. P. Christon,[7] M. Nosé,[8] H. U. Frey,[9] I. Shinohara,[1] T. Mukai,[1] Y. Saito,[1] and H. Hayakawa[1]

Received 30 March 2008; revised 19 September 2008; accepted 24 October 2008; published 22 January 2009.

[1] We have obtained a state-of-the-art picture of substorm-associated evolution of the near-Earth magnetotail and the inner magnetosphere for understanding the substorm triggering mechanism. We performed superposed epoch analysis of Geotail, Polar, and GOES data with 2-min resolution, utilizing a total of 3787 substorms for each of which auroral breakup was determined from Polar UVI or IMAGE FUV auroral imager data. The decrease of the north-south magnetic field associated with plasmoids and the initial total pressure decrease suggest that the magnetic reconnection first occurs in the premidnight tail, on average, at $X \sim -16$ to -20 R_E at least 2 min before auroral onset. The magnetic reconnection site is located near the tailward edge of a region of considerably taillike magnetic field lines and intense cross-tail current, which extends from $X \sim -5$ to -20 R_E in the premidnight sector. Then the plasmoid substantially evolves tailward of $X \sim -20$ R_E immediately after onset. Almost simultaneously with the magnetic reconnection, the dipolarization begins first at $X \sim -7$ to -10 R_E 2 min before onset. The dipolarization region then expands tailward as well as in the dawn-dusk directions and earthward. We find that the total pressure generally enhances in association with the dipolarization, with the contribution of high-energy particles. Also, energy release is more significant between the regions of the magnetic reconnection and the initial dipolarization. The present results will be helpful as a reference guide to developing the overall picture of magnetotail evolution and studying the causal relationship between the magnetic reconnection and the dipolarization as well as detailed mechanisms of each of the two processes on the basis of multispacecraft observations.

Citation: Miyashita, Y., et al. (2009), A state-of-the-art picture of substorm-associated evolution of the near-Earth magnetotail obtained from superposed epoch analysis, *J. Geophys. Res.*, *114*, A01211, doi:10.1029/2008JA013225.

1. Introduction

[2] Part of the energy of the solar wind enters into the magnetosphere when the interplanetary magnetic field (IMF) reconnects with the Earth's magnetic field at the dayside magnetopause. The solar wind input enhances during southward IMF periods. As a result, the energy accumulates in the form of distorted magnetic fields in the magnetotail, and the growth phase of the substorm begins. When this energy accumulates in excess or when external conditions change, a rapid catastrophic instability or reconfiguration occurs, causing significant release and dissipation of the stored energy, i.e., the substorm expansion onset. This loading-unloading process in the magnetotail plays an important role in causing substorms. During substorms various phenomena occur in the magnetosphere, in the ionosphere, and on the ground: plasmoid, bursty bulk flow, dipolarization, formation of the current wedges, energetic particle injection around geosynchronous orbit, auroral breakup, westward auroral electrojet, and Pi2 pulsation.

[3] The triggering mechanism of the substorm expansion onset has been a major issue in magnetospheric substorm research. Various models have been proposed. A principal candidate is the near-Earth neutral line (NENL) model [e.g., *Russell*, 1972, 1974; *Hones*, 1976; *Baker et al.*, 1996; *Shiokawa et al.*, 1997, 1998]. In this model, a neutral line is formed in the near-Earth tail or midtail, and the magnetic

[1]Institute of Space and Astronautical Science, Japan Aerospace Exploration Agency, Kanagawa, Japan.
[2]Department of Geophysics, Kyoto University, Kyoto, Japan.
[3]Research Institute for Sustainable Humanosphere, Kyoto University, Kyoto, Japan.
[4]Applied Physics Laboratory, Johns Hopkins University, Laurel, Maryland, USA.
[5]Solar-Terrestrial Environment Laboratory, Nagoya University, Nagoya, Japan.
[6]Institute of Geophysics and Planetary Physics, University of California, Los Angeles, California, USA.
[7]Focused Analysis and Research, Columbia, Maryland, USA.
[8]Data Analysis Center for Geomagnetism and Space Magnetism, Graduate School of Science, Kyoto University, Kyoto, Japan.
[9]Space Sciences Laboratory, University of California, Berkeley, California, USA.

0148-0227/09/2008JA013225$09.00

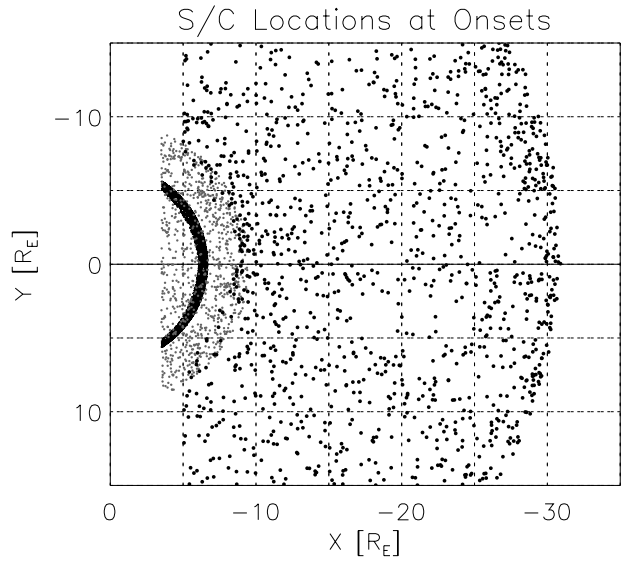

Figure 1. Locations of Geotail (larger black dots), Polar (smaller gray dots), and GOES (small black dots) at the substorm expansion onsets in GSM coordinates.

reconnection begins, resulting in the formations of the tailward-moving plasmoid and the earthward bursty bulk flow (BBF) which transport magnetic flux, mass, and energy at a high speed. The fast earthward flow causes the dipolarization in the near-Earth region. This model can naturally explain the plasmoid formation. However, it is still debatable whether or not earthward BBFs during a substorm are always intermittent and incapable of carrying magnetic fluxes and energy that are required for a substorm [*Angelopoulos et al.*, 1994]. Also, fast earthward flows are less frequently observed on the earthward side of the magnetic reconnection site than fast tailward flows associated with plasmoids on the tailward side [*Machida et al.*, 1999; *Miyashita et al.*, 2000, 2003]. The location of the magnetic reconnection site has been proposed by many previous studies: for example, $X < -20\ R_E$ [*Baumjohann et al.*, 1989], $X \sim -21\ R_E$ [*Baumjohann et al.*, 1999], $-20 > X > -30\ R_E$ in the premidnight sector [*Nagai et al.*, 1998], $X \sim -20\ R_E$ in the premidnight sector [*Machida et al.*, 1999; *Miyashita et al.*, 2000, 2003], and $X \sim -15$ to $-18\ R_E$ [*Slavin et al.*, 2002].

[4] Another principal candidate for substorm triggering mechanism is the current disruption (CD) model [e.g., *Lui*, 1996]. This model predicts that the ballooning instability [*Roux et al.*, 1991; *Bhattacharjee et al.*, 1998; *Cheng and Lui*, 1998] or the cross-field current instability [*Lui et al.*, 1991] causes the CD in a localized region of the plasma sheet at $X \sim -10\ R_E$, resulting in the dipolarization and the formation of the current wedges. The CD also generates a tailward-propagating rarefaction wave, which causes the magnetic reconnection in the midtail. The CD region expands tailward in the course of a substorm. The CD model has an advantage of explaining the location and timing of the auroral breakup [cf. *Samson et al.*, 1992], but it cannot necessarily account for the plasmoid formation as a natural consequence. The basic differences between the CD and NENL models are the location of the initial change and the propagation direction of the flow or wave.

[5] Other models proposed so far include the magnetosphere-ionosphere coupling model [*Kan et al.*, 1988; *Rothwell et al.*, 1988; *Kan*, 2007], the convection reduction model [*Lyons*, 1995], the boundary layer dynamics model [*Rostoker and Eastman*, 1987; *Rostoker*, 1996], and the thermal catastrophe model [*Smith et al.*, 1986; *Goertz and Smith*, 1989].

[6] For clarifying the causal relationship of substorm-associated processes in the magnetotail, it is helpful to employ a timing analysis, such as the superposed epoch analysis [e.g., *Lui et al.*, 1998; *Nagai et al.*, 1998; *Machida et al.*, 1999; *Miyashita et al.*, 2000, 2003]. Using plasma and magnetic field data from the Geotail spacecraft, *Machida et al.* [1999] and *Miyashita et al.* [2000, 2003] as well as *Nagai et al.* [1998] concluded that the magnetic reconnection plays a key role in substorm expansion triggering.

[7] In the present paper we have performed superposed epoch analyses more extensively than in our previous paper [*Miyashita et al.*, 2003]. The main differences are as follows: Increase of the number of the substorm events allows us to show the averages in *X*-*Y* bins. To reveal the initial dipolarization region, Polar and GOES data for the inner magnetosphere are used in addition to Geotail data; Polar can cover the region between the Geotail perigee, $\sim 9\ R_E$, and geosynchronous orbit. We consider the contribution of high-energy particles to the plasma pressure, which was neglected in the previous studies. Furthermore, we examined electric and magnetic field fluctuations with a low-frequency range below several Hz. The present paper shows the variations on the *X*-*Y* plane, while *Machida et al.* [2009] show those on the *X*-*Z* plane. Finally we discuss the causal relationship between the magnetic reconnection and the dipolarization as well as a few issues concerning the magnetic reconnection in the near-Earth magnetotail.

2. Data

[8] We utilized a total of 3787 substorm events determined from the auroral breakup: 1020 substorms from the Polar ultraviolet imager (UVI) [*Torr et al.*, 1995] from March 1996 to December 1999 [*Liou et al.*, 2000] and 2767 substorms from the IMAGE far ultraviolet imager (FUV) [*Mende et al.*, 2000a, 2000b, 2000c] from May 2000 to December 2005 [*Frey et al.*, 2004; *Frey and Mende*, 2007]. The substorm expansion onset times ($t = 0$) were determined with an accuracy of less than (Polar) or equal to (IMAGE) 2 min.

[9] For magnetospheric variations, we used data from the Geotail, Polar, and GOES 8, 9, 10, and 12 spacecraft. At least one of these spacecraft was located in the nightside sector during each of the selected events: the magnetotail in $-5 \geq X \geq -31\ R_E$ and $|Y| \leq 15\ R_E$ in GSM coordinates for Geotail, the inner magnetosphere and the magnetotail in $-3.5 \geq X \geq -10\ R_E$, $|Y| \leq 9\ R_E$, and $|Z| \leq 5\ R_E$ for Polar, and geosynchronous orbit in $-3.5 \geq X \geq -6.6\ R_E$ and $|Y| \leq 6\ R_E$ for GOES. The distribution of the locations of these spacecraft at the substorm onsets is shown in Figure 1; the

number of the data points are 1287 from Geotail, 917 from Polar, and 3466 from GOES. The coverage of the region is extensive enough to observe the dipolarization in addition to the magnetic reconnection and resultant plasmoid.

[10] We performed superposed epoch analyses of various parameters which are fundamental to the understanding of magnetotail dynamics as well as mass and energy transport. The parameters examined include the plasma flow, the north-south magnetic field, the dawn-dusk electric field, the magnetic and electric field fluctuations, the total pressure, and the mass and energy fluxes, although only some of them are shown in the present paper. The data mentioned below were averaged in 2-min intervals from 11 min before onset to 21 min after onset for each event. This time resolution is due to the time accuracy of the auroral onset times and yields an overall picture of magnetotail variations in an MHD scale.

[11] For the Geotail data, the ion moments, the magnetic field, and the electric field were measured by the energy-per-charge analyzer (EA) of the low-energy particle experiment (LEP) [*Mukai et al.*, 1994], the fluxgate magnetometer of the magnetic field experiment (MGF) [*Kokubun et al.*, 1994], and the double probe of the electric field detector (EFD-P) [*Tsuruda et al.*, 1994], respectively. The time resolution of these data is 12 s, which corresponds to a four-spin period. The ion moments were calculated from ions with an energy-per-charge range from a few tens of eV/q to $\sim$40 keV/q under the assumption that all ions are protons. For the ion pressure, we also used the data of energetic protons with an energy range of 44 to 265 keV, obtained from the suprathermal ion composition spectrometer (STICS) of the energetic particles and ion composition instrument (EPIC) [*Williams et al.*, 1994], to take into account the contribution from high-energy particles beyond the instrumental range of LEP.

[12] The classification of the Geotail data into the plasma sheet (PS), the plasma sheet boundary layer (PSBL), and the lobe was based on the ion β ($=NkT/(B^2/2\mu_0)$) [*Miyashita et al.*, 2000]: $\beta \geq \beta_1$ for the PS, $\beta_2 \leq \beta < \beta_1$ for the PSBL, and $\beta < \beta_2$ for the lobe, where the boundary value between the PS and the PSBL β_1 was defined as $\beta_1 = 1$ at $X \leq -15\ R_E$, and $\log_{10}\ \beta_1 = -0.14X - 2.1$ at $X > -15\ R_E$, and that between the PSBL and the lobe β_2 was defined as $\beta_2 = 0.05$ at $X \leq -15\ R_E$, and $\log_{10}\ \beta_2 = -0.14X - 3.4$ at $X > -15\ R_E$.

[13] For the near-Earth region, we used the magnetic field data obtained from the Polar magnetic field experiment (MFE) [*Russell et al.*, 1995] with 0.92-min resolution and from the GOES magnetometers with 1-min resolution.

3. Superposed Epoch Analyses

[14] In this section, we show the results of superposed epoch analyses of the plasma flow, the north-south magnetic field, the total pressure, the dawn-dusk electric field, and the magnetic and electric field fluctuations. The results of the mass and energy fluxes have been described in detail in the previous papers by *Miyashita et al.* [2001, 2003]. Here the data of the north-south magnetic field are from Geotail, Polar, and GOES, while those of the other parameters are only from Geotail. We used arithmetic averages, but the results essentially does not change even if median values are used, except for fast earthward flows.

[15] Figure 2 (left) shows two-dimensional plots of the X component of the plasma (ion) flow V_x in the PS and PSBL from 6 min before onset ($t = -6$ min) to 20 min after onset ($t = 20$ min). The data are averaged in 4 $R_E \times 4\ R_E$ bins in X and Y; the bins are slid by 2 R_E on the X-Y plane, so that only their central parts of 2 $R_E \times 2\ R_E$ are shown in Figure 2 not to overlap each other. The data of the PSBL are included, since the PSBL can have the characteristics of the PS according to our definition, and substorm-associated flows are also seen in the PSBL. The times shown in Figure 2 and the text below are the centers of the averaging intervals. Note that we plotted the bin averages in the present study, while 2-min data themselves were all plotted in our previous papers [*Miyashita et al.*, 2000, 2001, 2003]. Figure 3 (left) shows the Y component of the plasma flow V_y in the PS and PSBL.

[16] Before and at $t = -4$ min there are fast earthward flows at a speed of $>\sim$100 km/s at $X < -15\ R_E$, probably generated in the distant tail. More fast earthward flows appear at $X < -12\ R_E$ after $t = -2$ min, but they are not distributed very widely even immediately after onset (Figure 2). This is probably due to the localization of the flows in the Y direction as well as in the Z direction [*Angelopoulos et al.*, 1997; *Nakamura et al.*, 2004]. The V_y component generally has duskward and dawnward speeds of $\sim$40 km/s in the premidnight and postmidnight sectors, respectively, at $X < -12\ R_E$ (Figure 3), indicating that the fast earthward flows slightly deflect toward the tail flanks. Meanwhile, fast earthward flows are not seen in the near-Earth region at $X > -12\ R_E$ around onset, although earthward flows slightly grow at $t = 2$ min at $(X, Y) \sim (-8, 0)$ R_E (Figure 2), where there are very slow flows and even tailward flows [see *Miyashita et al.*, 2000, 2003]. Taking into account the V_y component, the plasma flows in the near-Earth region of $Y > -4\ R_E$ are slow, $\sim$40 km/s, and largely deflect duskward around onset. The duskward component seems to weaken after $t = 4$ min. (If the median values are taken instead of the averages, earthward flows are seen to be slow. This is because the observation frequency of fast earthward flows is not very high, so that slow flows tend to be taken as median values [cf. *Miyashita et al.*, 2003, Figure 1].)

[17] On the other hand, fast tailward flows begin to grow significantly in the premidnight sector at $X < -20\ R_E$ at onset ($t = 0$), associated with the formation and evolution of

Figure 2. Two-dimensional plots of the (left) X component of the plasma (ion) flow V_x on the GSM X-Y plane in the plasma sheet (PS) and the plasma sheet boundary layer (PSBL); the (middle) deviation of the north-south magnetic field ΔB_z in the PS, PSBL, and lobe; and the (right) normalized total pressure deviation $\Delta P_t/\overline{P_t}$ in the PS, PSBL, and lobe (a) from $t = -6$ to 6 min and (b) from $t = 8$ to 20 min. The size of the bins is 4 $\times$ 4 R_E, except for ΔB_z in the inner magnetospheric region that Polar and GOES cover, 2 $R_E \times 2\ R_E$. The 4 $\times$ 4 R_E (2 $\times$ 2 R_E) bins are slid by 2 R_E (1 R_E) on the X-Y plane so that only their central parts of 2 $\times$ 2 R_E (1 $\times$ 1 R_E) are shown not to overlap each other. The times shown are the centers of the averaging intervals.

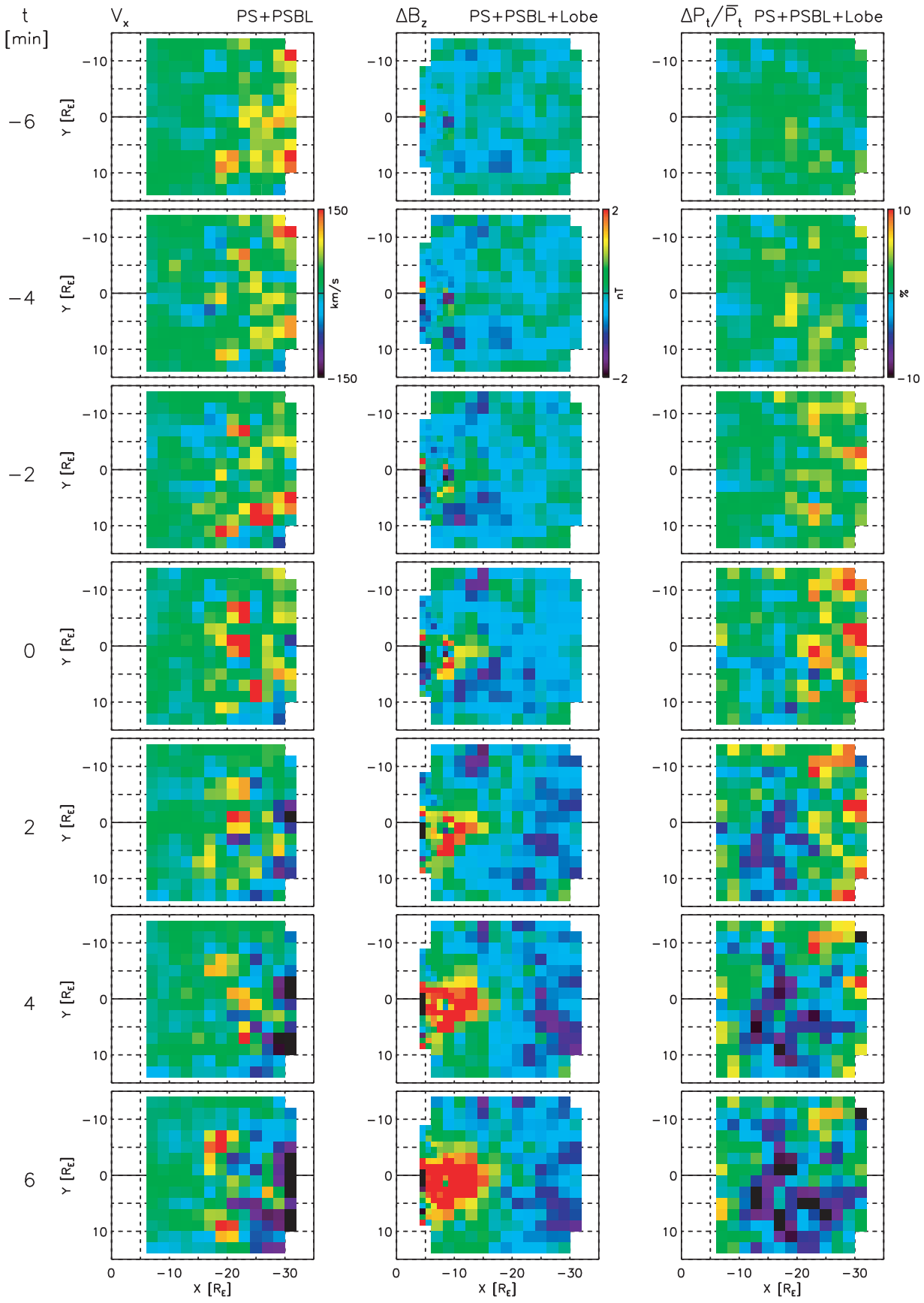
t [min]
V_x PS+PSBL
ΔB_z PS+PSBL+Lobe
$\Delta P_t/\bar{P}_t$ PS+PSBL+Lobe
−6
−4
−2
0
2
4
6
Y [R_E]
X [R_E]
150
−150
km/s
2
−2
nT
10
−10
%

Figure 2

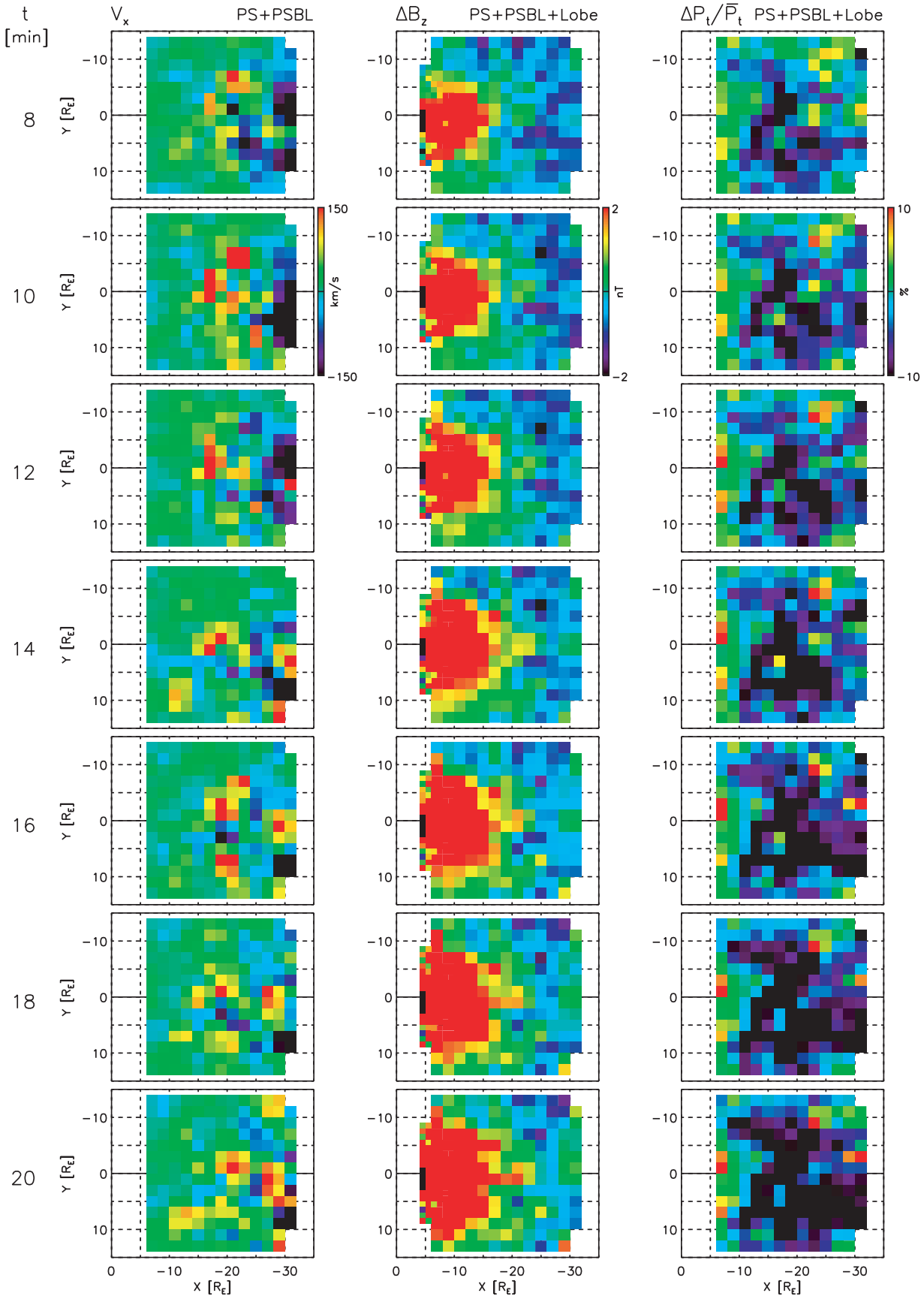

Figure 2. (continued)

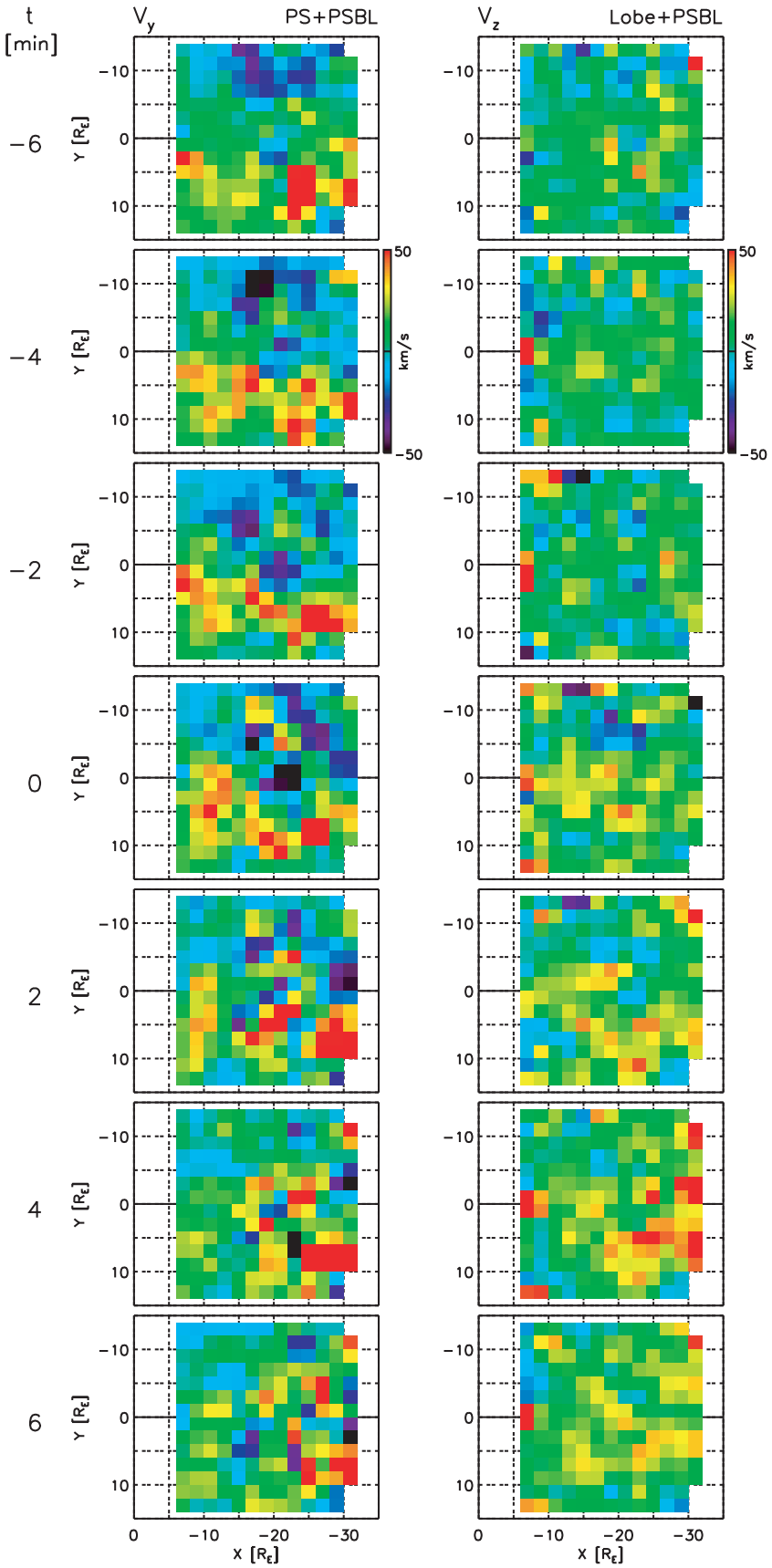

Figure 3. Two-dimensional plots of the (left) Y component of the plasma flow V_y in the PS and PSBL and the (right) Z component of the plasma flow V_z in the lobe and PSBL in 4×4 R_E bins from $t = -6$ to 6 min. The positive V_z is directed toward the PS, and the negative V_z is directed toward the lobe.

the plasmoid. The flow speed at $X < -25\ R_E$ then exceeds a few hundred km/s. The speed at $-20 > X > -25\ R_E$ is somewhat slower, possibly because the flows are not accelerated sufficiently in this region, and the plasma sheet is so thin that fast flows are missed in observations. The region of fast tailward flow successively expands duskward and dawnward from the premidnight sector at $Y \sim 2\ R_E$, accompanied by duskward and dawnward flow components of $>\sim$50 km/s, respectively; this corresponds to the expansion of the plasmoid [*Ieda et al.*, 1998; *Slavin et al.*, 1999]. The wide distribution of the fast tailward flows is in remarkable contrast to the localization of the fast earthward flows. The fast tailward flows are quenched after $t = 10$ min.

[18] Figure 3 (right) shows the Z component of the plasma flow V_z toward the PS in the lobe and PSBL. In general, V_z is directed toward the PS in the entire tail throughout the interval. At onset V_z toward the PS begins to enhance over a wide area of $-7 > X > -30\ R_E$ and $-4 < Y < 8\ R_E$ and then enhances in the entire tail. In particular, V_z toward the PS is large in the premidnight sector at $X < -20\ R_E$. The enhancement at $X \sim -10\ R_E$ is associated with the dipolarization, while that at $X < -20\ R_E$ is associated with the progress of the magnetic reconnection and is seen after the plasmoid passage [*Taguchi et al.*, 1998; *Slavin et al.*, 1999; *Miyashita et al.*, 2000].

[19] Figure 2 (middle) shows the deviation of the north-south magnetic field, $\Delta B_z(t) = B_z(t) - \overline{B_z}$, in the PS, PSBL, and lobe, where $\overline{B_z}$ was defined as the average value over the interval from $t = -11$ to -7 min, calculated for each event. Here the size of bins is reduced to $2\ R_E \times 2\ R_E$ for the inner magnetospheric region that Polar and GOES cover. For checking the timing of the changes in more detail, Figure 4 (Figure 5) shows the time profiles of ΔB_z in the PS, PSBL, and lobe for the $4\ R_E \times 4\ R_E$ ($2\ R_E \times 2\ R_E$) bins of $-5 \geq X \geq -31\ R_E$ and $-5 \leq Y \leq 9\ R_E$ ($-4.5 \geq X \geq -10.5\ R_E$ and $-0.5 \leq Y \leq 6.5\ R_E$) shown in Figure 2. The asymmetric Y range with respect to midnight is due to the dawn-dusk asymmetry of the substorm-associated changes, as shown in Figure 2 [see also *Nagai et al.*, 1998; *Ieda et al.*, 1998].

[20] The negative ΔB_z gradually grows in the entire tail before onset, corresponding to the change to a more taillike magnetic field. In particular, the relatively large negative ΔB_z appears in the premidnight sector at $X \sim -5$ to $-20\ R_E$ and $Y \sim 2$ to $12\ R_E$ before onset, as seen in Figure 2. This implies that magnetic field lines become considerably taillike and the cross-tail current is significantly intensified there before onset, as suggested by *Pulkkinen et al.* [1999] and *Pulkkinen and Wiltberger* [2000]. At onset the negative ΔB_z substantially grows, i.e., B_z decreases in the premidnight sector tailward of $X \sim -20\ R_E$ (Figure 2). (We found that the elevation angle has a larger decrease tailward of $X \sim -20\ R_E$ after onset than earthward of $X \sim -20\ R_E$ before onset.) From Figure 4 (right), the development of the negative ΔB_z already begins 2 min before onset for $X < -23\ R_E$. In some bins, this change seems to begin 4 min before onset. In this region the fast tailward flows are seen, as shown in Figure 2 (left), so that the negative ΔB_z is associated with the plasmoid in the PS and the traveling compression region (TCR) in the PSBL and the lobe. Corresponding to the plasmoid expansion, the region of the growing negative ΔB_z expands both duskward and dawnward from $Y \sim 2\ R_E$. The negative ΔB_z is quenched after $t = -10$ min.

[21] On the other hand, simultaneously with the plasmoid evolution, the positive ΔB_z begins to grow, i.e., B_z substantially increases first at $X \sim -7$ to $-10\ R_E$ and $Y \sim 4\ R_E$ 2 min before onset in association with the dipolarization, as seen in Figure 2 (middle), Figure 4 (left), and Figure 5. Note that fast earthward flows do not appear in this region, as shown in Figure 2 (left). The dipolarization region then successively expands tailward, duskward, dawnward, and earthward, which is consistent with the finding that the auroral bulge and dipolarization regions are closely related [*Liou et al.*, 2002]. The dipolarization region reaches $X \sim -17\ R_E$ at $t \sim 6$ min, $Y \sim 10\ R_E$ at $t \sim 2$ min, $Y \sim -5\ R_E$ at $t \sim 2$ min, and $X \sim -5\ R_E$ at $t \sim 0$ min. These correspond to a tailward expansion speed of $\sim$100 km/s, roughly consistent with *Jacquey et al.* [1991], *Ohtani et al.* [1992], and *Baumjohann et al.* [1999], duskward and dawnward speeds of $\sim$200 km/s [*Nagai*, 1982; *Liou et al.*, 2002], and an earthward speed of $\sim$200 km/s [*Ohtani*, 1998]. It should be noted that the location of the initial dipolarization is clearly shown in the present study by combining the Polar and GOES data taken earthward of the Geotail perigee of $\sim 9\ R_E$, while the Polar and GOES data were not included in our previous studies.

[22] Figure 2 (right) shows the normalized deviation of the total pressure $\Delta P_t/\overline{P_t}(t = -11$ to -7 min) in the PS, PSBL, and lobe, where $\Delta P_t(t) = P_t(t) - \overline{P_t}(t = -11$ to -7 min). The total pressure is the sum of the ion thermal and magnetic pressures ($P_t = NkT + B^2/2\mu_0$). Here the contribution from high-energy particles beyond the instrumental range of Geotail LEP ($>\sim$40 keV/q), which was neglected in our previous studies, was considered by combining the Geotail LEP and EPIC-STICS data. The contribution from electrons was neglected. Figure 6 shows the time profiles of $\Delta P_t/\overline{P_t}$ for the $4\ R_E \times 4\ R_E$ bins in the same format as Figure 4.

[23] Before and at $t = -4$ min, the positive $\Delta P_t/\overline{P_t}$ enhances, that is, the total pressure increases in the entire tail. At $t = -2$ min, however, the values of the positive $\Delta P_t/\overline{P_t}$ become small in the premidnight sector at $X \sim -16$ to $-20\ R_E$ and $Y \sim 0$ to $5\ R_E$, followed by the appearance and growth of the negative $\Delta P_t/\overline{P_t}$, as shown in Figure 2 (right) and Figure 6 (middle). Namely, it is confirmed that the total pressure decrease occurs first in this region. This change relates to the magnetic reconnection [*Miyashita et al.*, 1999, 2000]. Subsequently the total pressure also decreases in the surrounding regions, except the dipolarization region, at or immediately after onset; the negative $\Delta P_t/\overline{P_t}$ gradually grows, that is, the total pressure decreases in the entire tail.

[24] In contrast, the total pressure generally increases, rather than decreases, in the near-Earth region of $X > -10\ R_E$ and $-5 < Y < 8\ R_E$ simultaneously with or a few minutes after the beginning of the dipolarization, except for the bin of $X = -7\ R_E$ and $Y = 1\ R_E$ (Figure 2, right and middle, as well as Figure 4, left, and Figure 6, left). Outside this region, particularly tailward of $X \sim -10\ R_E$, the total pressure decreases just before or after onset, i.e., before the dipolarization region reaches there, as mentioned above; when the dipolarization occurs, the total pressure continues to decrease or begins to increase.

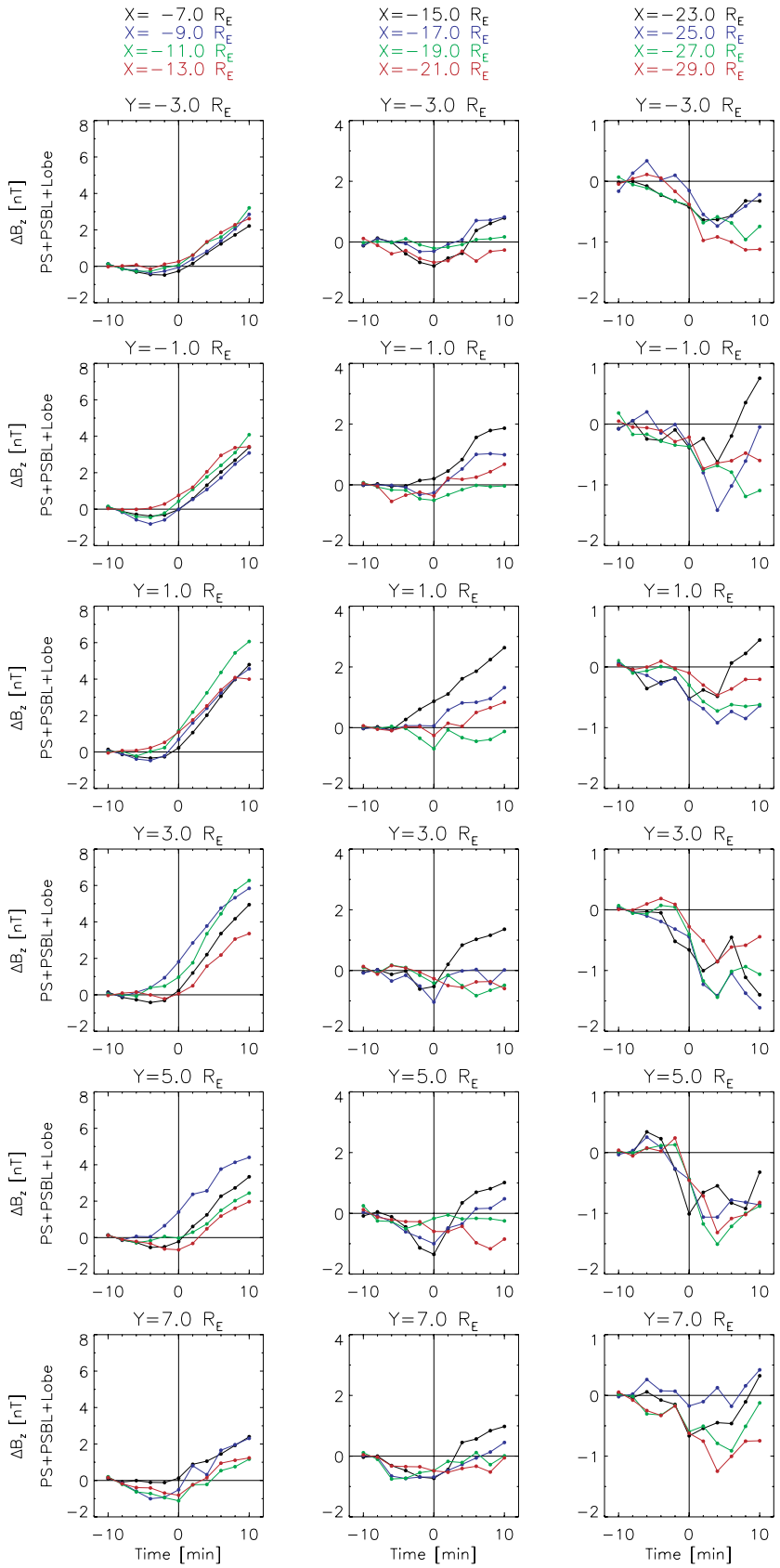

Figure 4. Time profiles of the deviation of the north-south magnetic field ΔB_z in the PS, PSBL, and lobe for the 4×4 R_E bins of $-5 \geq X \geq -31$ R_E and $-5 \leq Y \leq 9$ R_E shown in Figure 2. The X and Y locations indicated are the centers of the bins. Different colors of the lines correspond to different X distances indicated at the top.

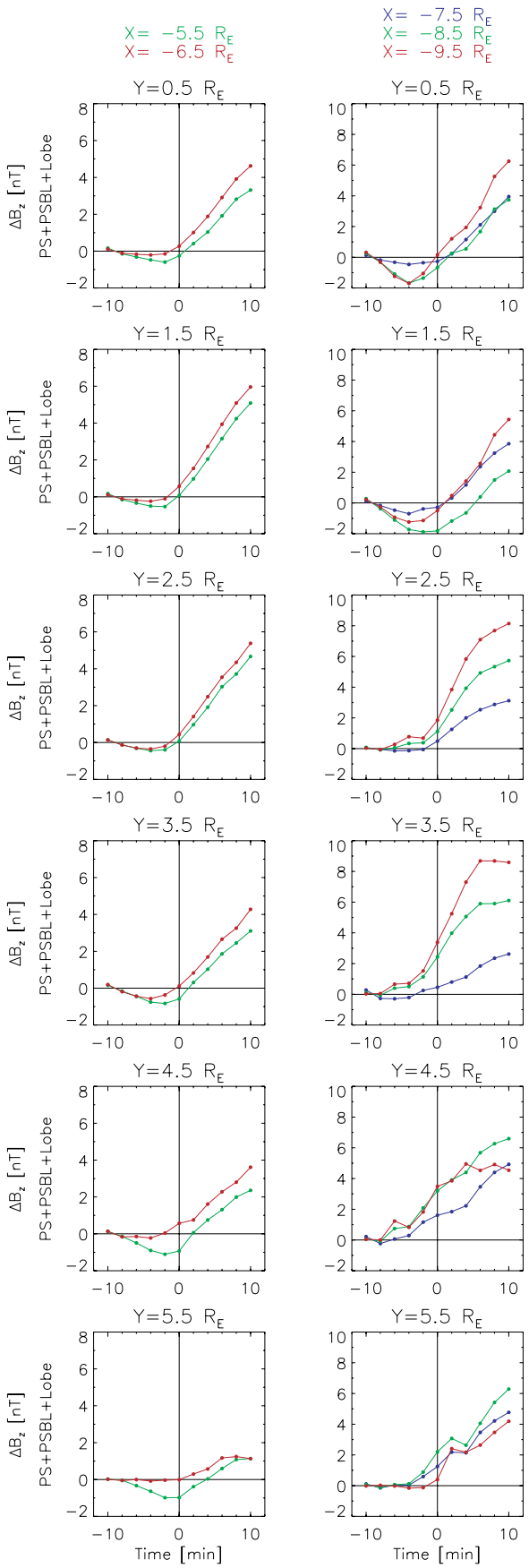

Figure 5. Time profiles of the deviation of the north-south magnetic field ΔB_z in the PS, PSBL, and lobe for the $2 \times 2\ R_E$ bins of $-4.5 \geq X \geq -10.5\ R_E$ and $-0.5 \leq Y \leq 6.5\ R_E$ shown in Figure 2, in the format similar to Figure 4.

[25] Then we further examined in detail the ion and magnetic pressures in the plasma sheet. In $X > -10\ R_E$ and $-2 < Y < 6\ R_E$, the ion pressure increases in association with the dipolarization, which mainly results from the contribution of high-energy particles above 44 keV measured by Geotail EPIC-STICS, or energetic particle injection [see also *Kistler et al.*, 1992]. The ion pressure from low-energy particles below ~40 keV/q measured by Geotail LEP decreases or increases. The magnetic pressure generally decreases in this region (not shown). The result of the ion pressure is obviously different from those of *Lui et al.* [1992], who reported that the ion pressure in the plasma sheet decreases in association with the dipolarization. The pressure change due to low-energy particles can be explained by the results of *Lyons et al.* [2003]. They showed that low-energy particle fluxes decrease in association with the dipolarization, while high-energy particle fluxes increase; the transition from decrease to increase occurs at an energy between several and a few tens of keV, i.e., within the instrumental range of LEP. Further details about pressure changes associated with the dipolarization will be reported in a separate paper.

[26] The initial total pressure decrease occurs at $X \sim -16$ to $-20\ R_E$, but the absolute value of the total pressure decrease is more significant closer to the Earth, as shown in Figure 7 (right) for the total pressure deviation ΔP_t. The negative ΔP_t grows larger in the premidnight sector at $-10 > X > -20\ R_E$, particularly at $X \sim -12$ to $-18\ R_E$, than in the surrounding regions. Namely, energy release is more significant between the regions of the initial total pressure decrease and the initial dipolarization.

[27] Furthermore, we examined the total pressure itself P_t. As clearly shown in Figure 7 (left), the total pressure becomes larger on approaching the Earth. It enhances in $-10 > X > -18\ R_E$ and $2 < Y < 8\ R_E$ before onset in particular. This indicates the presence of more intense cross-tail currents, since the square root of the total pressure is nearly proportional to the lobe magnetic field under taillike condition. This region agrees with that of considerably taillike magnetic field lines and the larger decrease in the total pressure.

[28] We also examined the dawn-dusk electric field E_y, calculated from the frozen-in relation $\mathbf{E} = -\mathbf{V} \times \mathbf{B}$ using the data of the ion velocity and the magnetic field. As shown in Figure 8, E_y is generally directed duskward in the entire tail at $t = -6$ min and is large in the lobe and PSBL at $(X, Y) \sim (-17, 3)\ R_E$ and in the PS, PSBL, and lobe at $(X, Y) \sim (-8, 2)\ R_E$ in particular. At $t = -4$ min E_y in the lobe and PSBL enhances first at $-8 > X > -18\ R_E$ and then enhances successively in the surrounding regions; it enhances at $X < -20\ R_E$ just after onset. These variations in the lobe and PSBL relate to enhancements of the plasma flow and the Poynting flux toward the PS (see *Miyashita et al.* [2000, 2003], *Machida et al.* [2009], and Figure 3). Just after onset E_y in the PS enhances in the premidnight sector at $X \sim -10$ and $-30\ R_E$, associated with the dipolarization and the

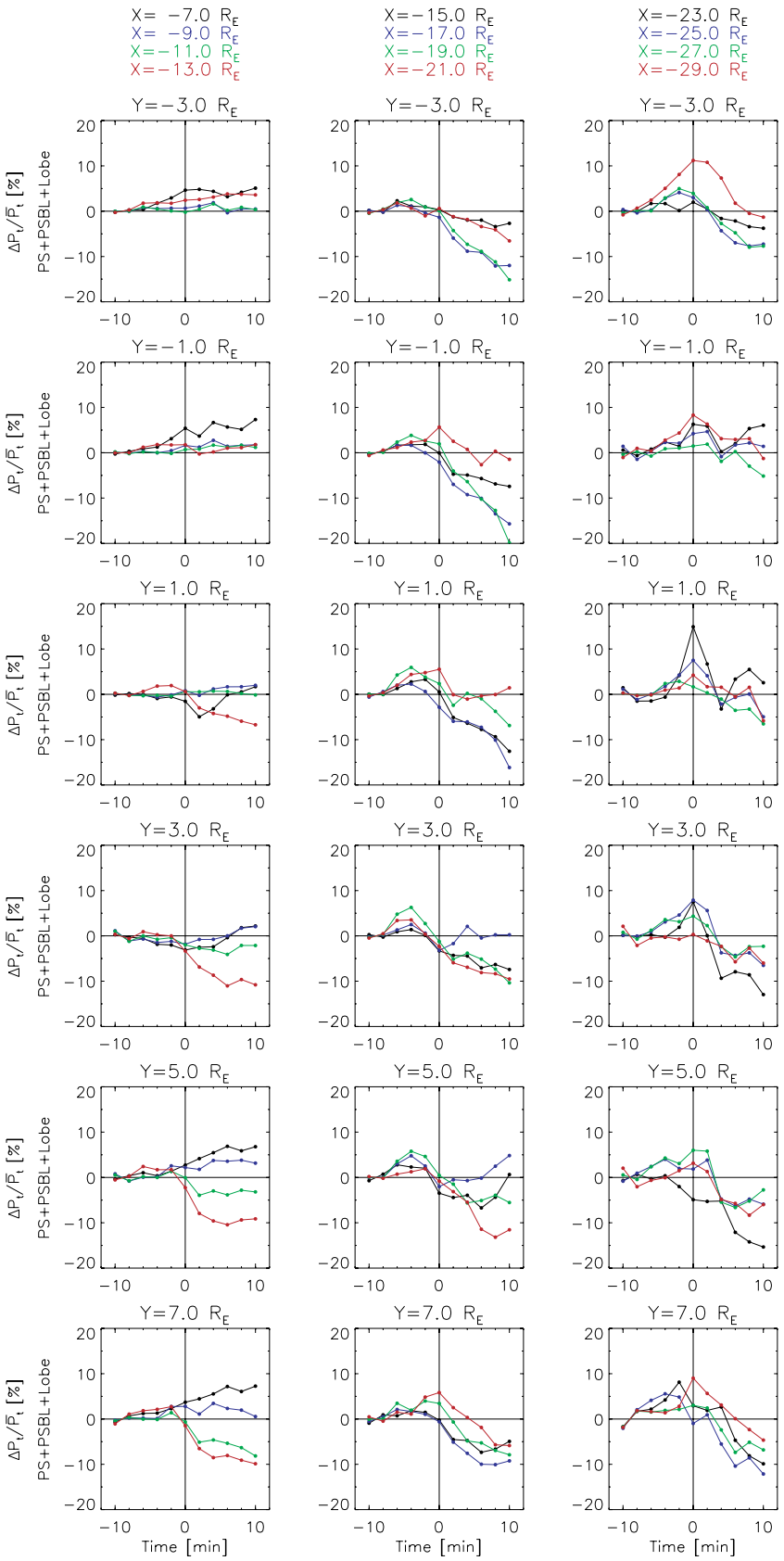

Figure 6. Time profiles of the normalized total pressure deviation $\Delta P_t/\overline{P_t}$ in the PS, PSBL, and lobe for the 4 × 4 R_E bins shown in Figure 2, in the same format as Figure 4.

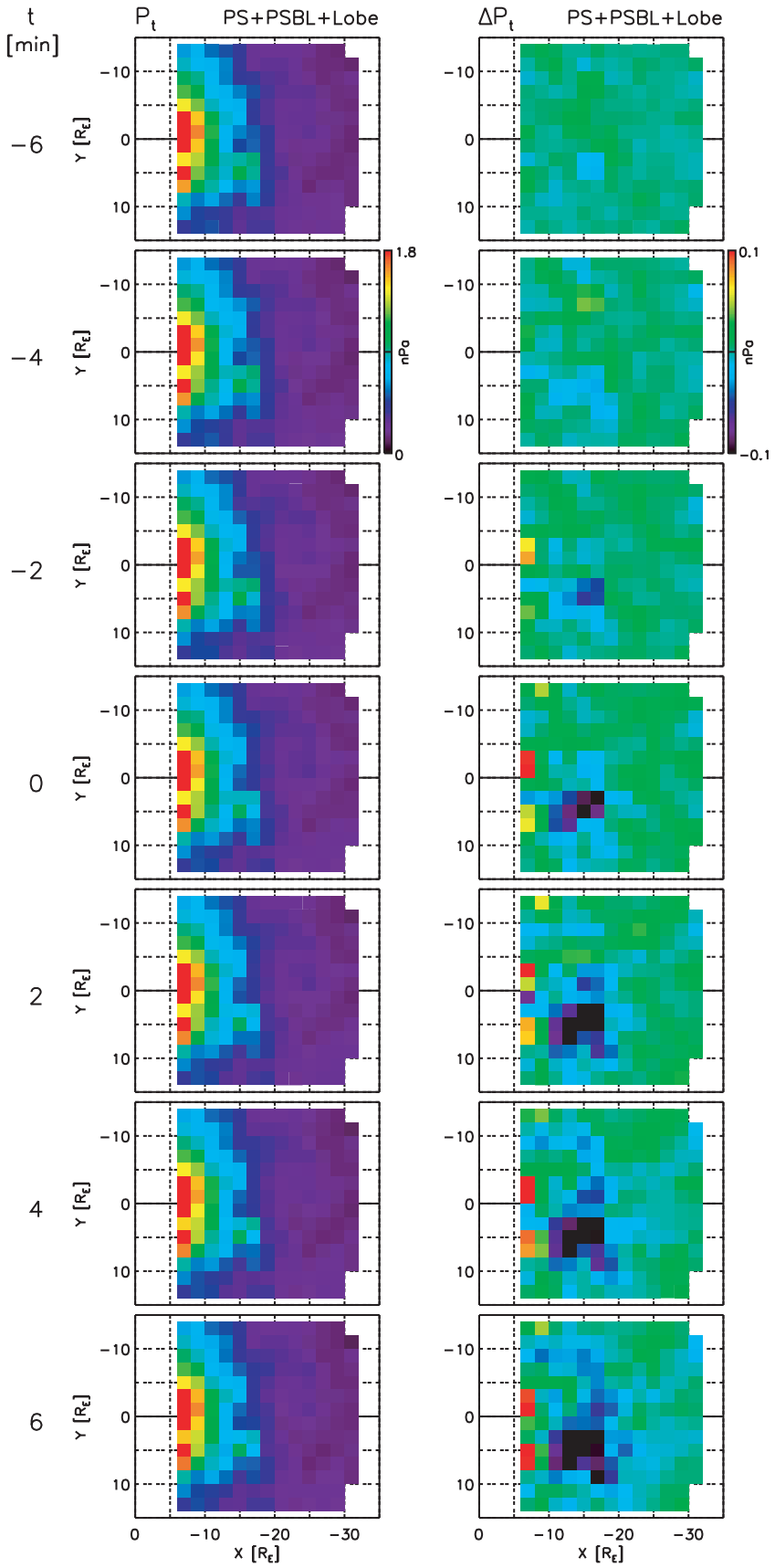

Figure 7. Two-dimensional plots of the (left) total pressure P_t and the (right) total pressure deviation ΔP_t in the PS, PSBL, and lobe in 4 × 4 R_E bins from $t = -6$ to 6 min.

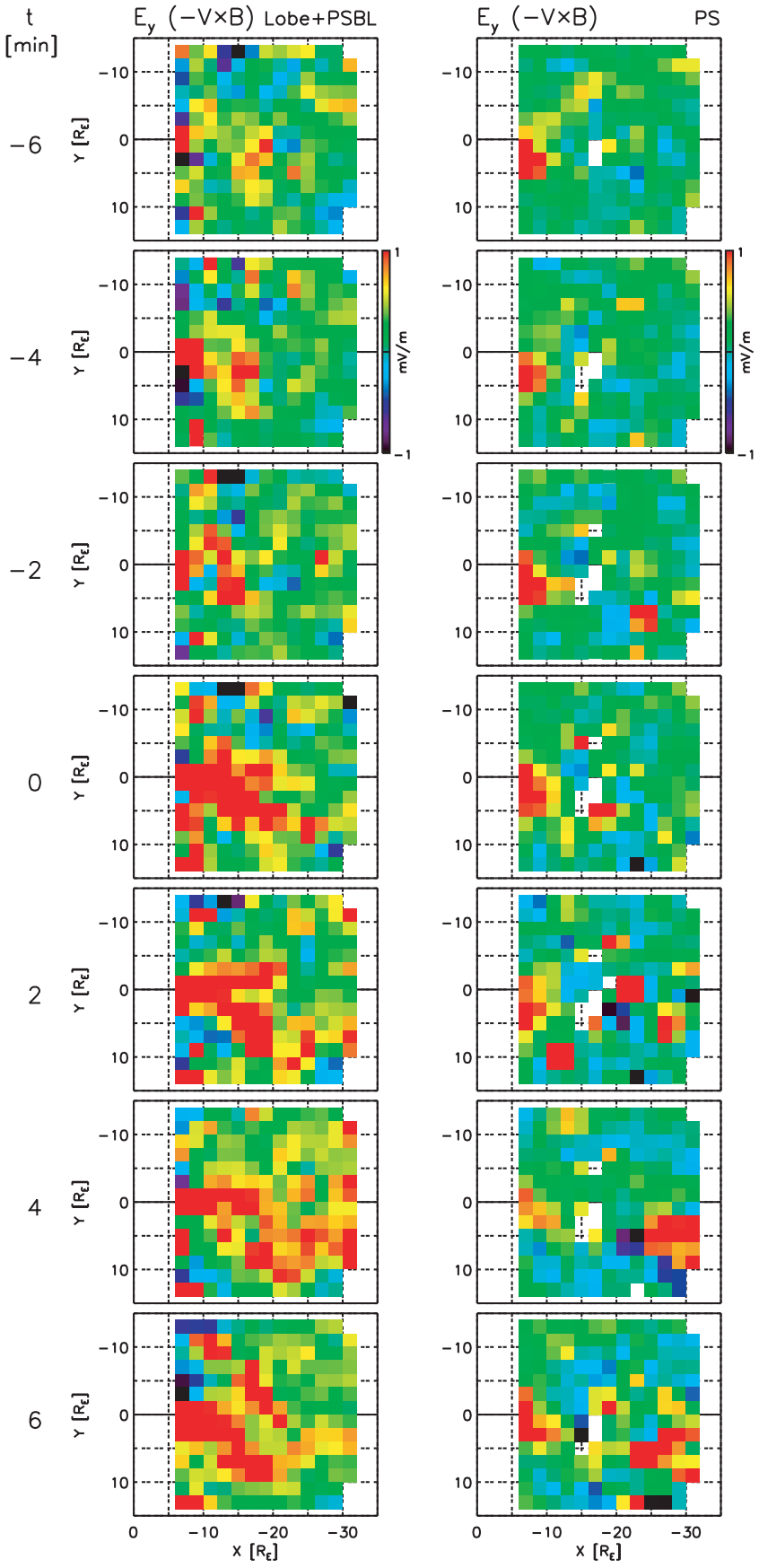

Figure 8. Two-dimensional plots of the dawn-dusk electric field E_y (left) in the lobe and PSBL and (right) in the PS in 4 × 4 R_E bins from $t = -6$ to 6 min. The electric field was calculated by $\mathbf{E} = -\mathbf{V} \times \mathbf{B}$.

plasmoid, respectively; E_y develops also in the PS at $X \sim -16$ to -20 R_E after onset, although some fluctuations are seen.

[29] The distribution of the enhanced E_y is evidently different between the lobe and the PS; that is, the enhanced E_y is widely distributed in the lobe and PSBL, while it is localized in the PS. This is because enhanced plasma flows toward the PS are seen in a wide area of the lobe and PSBL (Figure 3), while fast earthward flows in the PS are localized. The dipolarization at $X \sim -10$ R_E also causes the E_y enhancement but does not seem to make a large difference between the lobe and the PS.

[30] Here we also compared the deviation of E_y in the PS calculated from the frozen-in relation with that directly measured by the double probe of Geotail EFD and found that they vary in a similar way (not shown here, but see *Miyashita et al.* [2000, 2003]). Note that since 2 min averaged values were used in the present study, it is possible that rapid variations are averaged out even if the amplitude is very large. Most of ions are probably unmagnetized under rapid fluctuations or in the thin current sheet, that is, the frozen-in condition is broken in the magnetic reconnection [*Runov et al.*, 2003; *Asano et al.*, 2004] and dipolarization regions [*Lui*, 1996; *Lui et al.*, 1999], so that other terms of the generalized Ohm's law, such as the anomalous resistivity and Hall terms, may be important there [*Lui et al.*, 2007].

[31] Figure 9 shows the root mean squares (RMS) of the magnetic and electric fields in the PS, which are obtained from the 16 and 32 Hz sampling raw data, respectively. In the present study the root mean squares are used as measures of fluctuations with a low-frequency range below several Hz, although they can also become large even if the DC fields change. It is noticed that the root mean squares of both magnetic and electric fields become large in the premidnight sector at $X \sim -14$ to -20 R_E just before and after onset. They also develop at $X \sim -10$ and -30 R_E just after onset in relation to the dipolarization and the plasmoid, respectively. The details of these fluctuations should be investigated in the future.

4. Summary and Discussion

[32] We have performed the superposed epoch analyses of the substorm-associated evolution of the magnetotail and the inner magnetosphere, using the Geotail, Polar, and GOES data. Significant results are summarized in Figure 10 and as follows: The north-south magnetic field begins to decrease 2 or possibly 4 min before onset tailward of $X \sim -20$ R_E, associated with plasmoids and TCRs. Fast tailward flows substantially develop just after onset there. At $X > -20$ R_E, a few fast earthward flows are seen around onset and seem to reach only $X \sim -12$ R_E; plasma flows in the near-Earth region of $X > -12$ R_E and $Y > -4$ R_E are slow and largely deflect duskward. Almost simultaneously with the plasmoid formation and evolution, the north-south magnetic field begins to increase first at $X \sim -7$ to -10 R_E 2 min before onset in conjunction with the dipolarization. This location is at or just earthward of the Geotail perigee of $\sim$9 R_E and tailward of geosynchronous orbit. Then the dipolarization region successively expands tailward as well as duskward, dawnward, and earthward. The total pressure begins to decrease first in the premidnight tail at $X \sim -16$ to -20 R_E 2 min before onset and then decreases in the surrounding regions successively, whereas it generally increases in the near-Earth region at $X > -10$ R_E in association with the dipolarization, with the contribution of high-energy particles. The absolute value of the total pressure decrease is larger between the regions of the initial total pressure decrease and the initial dipolarization. The electric and magnetic field fluctuations appear at $X \sim -14$ to -20 R_E just before onset. The location of the initial total pressure decrease as well as the electric and magnetic field fluctuations corresponds to the tailward edge of a region of considerably taillike magnetic field lines and intense cross-tail current, which extends from $X \sim -5$ to -20 R_E in the premidnight sector.

[33] The particularly important, new findings of the present study are the initial location of the dipolarization region, the increase in the total pressure in association with the dipolarization, and the considerable decrease in the total pressure at $-12 > X > -18$ R_E. The former two were obtained by combining the magnetic field data measured by Polar and GOES between the Geotail perigee and geosynchronous orbit and by considering the contribution of high-energy particles to the plasma pressure.

[34] The observational results suggest that the magnetic reconnection first occurs in the premidnight tail, on average, at $X \sim -16$ to -20 R_E at least 2 min before onset. The further significant growth of the negative ΔB_z due to the plasmoid is seen tailward of $X \sim -20$ R_E in the premidnight tail, which begins 2 or possibly 4 min before onset (Figure 2). The initial total pressure decrease at $X \sim -16$ to -20 R_E 2 min before onset is interpreted as a result of the magnetic reconnection. The magnetic reconnection site is located near the tailward edge of a region of considerably taillike magnetic field lines and intense cross-tail current, which extends from $X \sim -5$ to -20 R_E in the premidnight sector. Then the plasmoid substantially evolves tailward of $X \sim -20$ R_E immediately after onset. Almost simultaneously with the magnetic reconnection (with 2-min resolution), the dipolarization begins first at $X \sim -7$ to -10 R_E 2 min before onset. The dipolarization region then expands tailward as well as in the dawn-dusk directions and earthward.

[35] There is no doubt that both of the magnetic reconnection and the dipolarization occur at different distances within a few minutes of the substorm expansion onset and play an important role in the change of the magnetotail structure, i.e., the plasmoid formation and the change from taillike to dipole-like configuration. Figure 11 shows two individual cases in which the plasmoid and the dipolarization were observed by Geotail in the midtail and by GOES 9 in the near-Earth tail, respectively, at the same time of the substorm onsets or the auroral breakups. (For the 25 February 1997 event, a slight increase of B_z observed by GOES 9 $\sim$3 min before the substorm onset probably correspond to a pseudobreakup at $\sim$0935 UT; B_z began to further increase at the substorm onset.) These events, as well as those shown by *Slavin et al.* [2002], indicate that both of the magnetic reconnection and the dipolarization do occur, and the resultant plasmoid and the dipolarization can be observed almost simultaneously at substorm onsets, consistent with the present statistical results. We should note that the initial magnetic reconnection and the initial dipolarization should have occurred a few minutes before

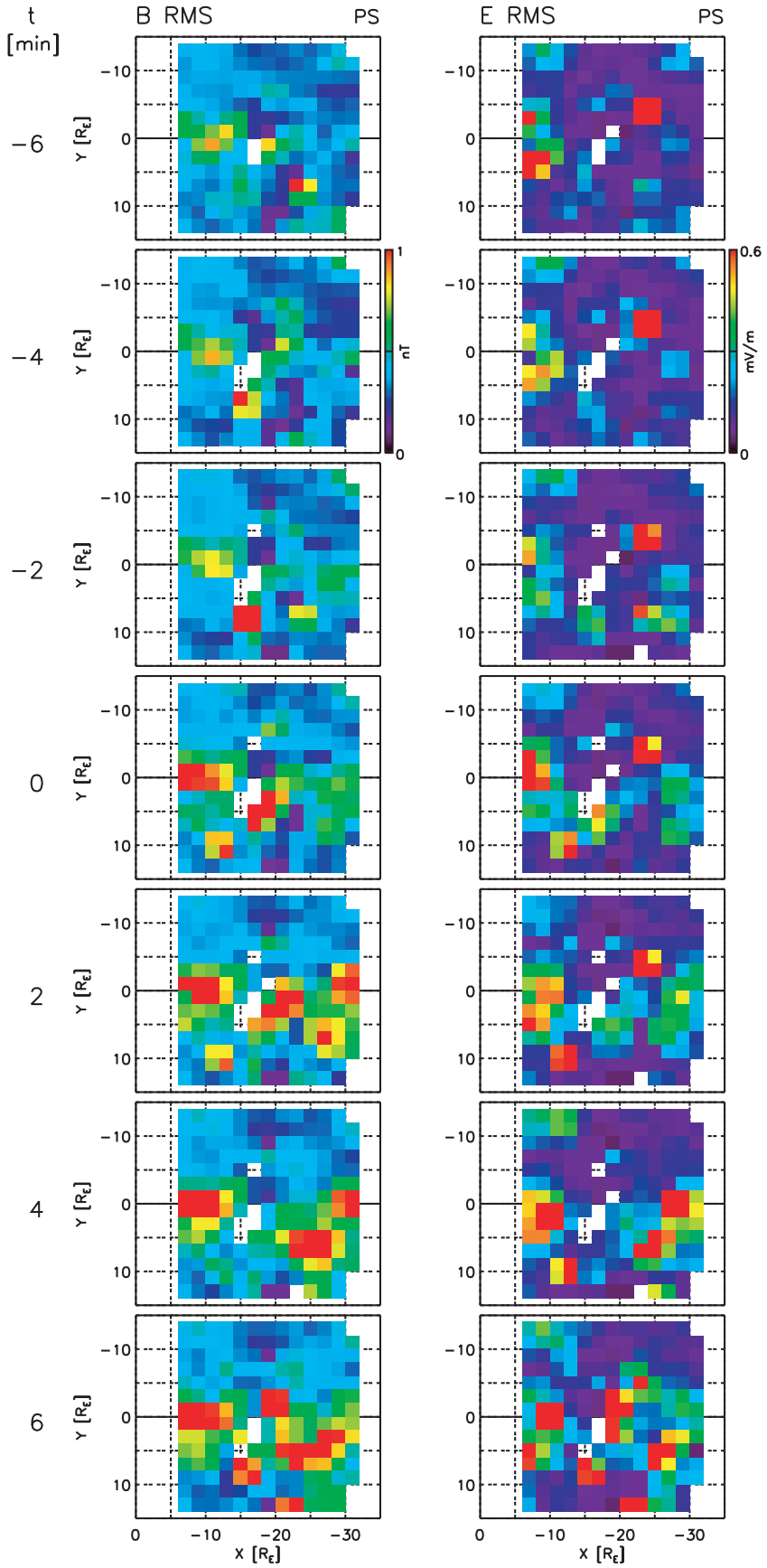

Figure 9. Two-dimensional plots of the root mean squares (RMS) of the (left) magnetic field and the (right) electric field in the PS in 4 × 4 R_E bins from $t = -6$ to 6 min.

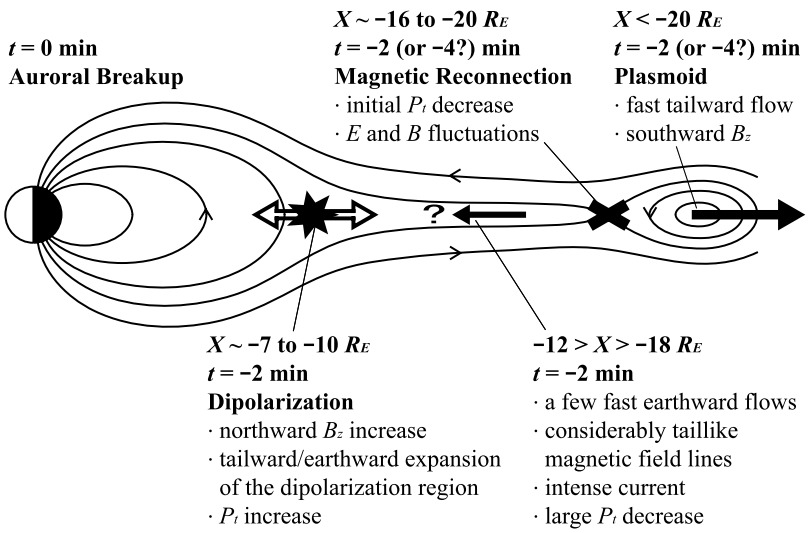

Figure 10. Summary of the statistical results. It is not exactly scaled.

the observations, since it is necessary to consider the propagation times due to the earthward and tailward flows generated by the magnetic reconnection, the rarefaction wave generated by the dipolarization, the plasmoid expansion in the Y direction, and the radial and azimuthal expansion of the dipolarization region. Better events should be obtained from more spacecraft, such as THEMIS, to investigate more detailed timing.

[36] A crucial issue is the causal relationship between the two processes. As a scenario in which one causes the other, for example, *Shiokawa et al.* [1997, 1998] proposed that the braking of fast earthward flows generated by the magnetic reconnection causes the dipolarization in the near-Earth tail. However, the behavior of the earthward flow is still unclear from the present statistical results. Fast earthward flows do not appear significantly around onset, probably due to their localization in the Y and Z directions in contrast to fast tailward flows, although the pairs of the fast earthward flow and the fast tailward flow/plasmoid were observed in some cases [*Petrukovich et al.*, 1998; *Slavin et al.*, 2002; *Angelopoulos et al.*, 2008]. Fast earthward flows seem to reach only $X \sim -12\ R_E$, not $X \sim -8\ R_E$ where the initial dipolarization takes place, which is consistent with the statistical result of *Shiokawa et al.* [1997]. *Ohtani et al.* [2006] and *Takada et al.* [2006] showed similar results, although nonsubstorm events may be included in their events. Also, according to the present results, E_y or the magnetic flux transport in the PS does not seem to be continuous between $X \sim -10$ and $-15\ R_E$ (Figure 8), in contrast to the result of *Schödel et al.* [2001], although nonsubstorm times may be included in their analysis. Thus it should be clarified whether or not the braking of the fast earthward flow directly causes the near-Earth dipolarization and, if not, whether or not some types of wave generated by the magnetic reconnection triggers the dipolarization.

[37] *Pu et al.* [1999, 2001] proposed another model that relates the fast flow and the current disruption (also discussed by *Zhang et al.* [2007] and *Cao et al.* [2008]). When a fast earthward flow generated by the magnetic reconnection in the midtail or other processes is braked, plasmas are compressed and pushed earthward. This can result in a rapid growth of the ballooning instability in the near-Earth region. Flow shear or a duskward flow can also set up a favorable condition for the ballooning instability. *Saito et al.* [2008] showed that ballooning mode waves occur at the high-β magnetic equator of the near-Earth tail a few minutes before dipolarization in the presence of the duskward flow. It should be further studied, however, how the ballooning mode waves are generated and relate to the onsets of the dipolarization and the substorm expansion.

[38] In contrast, *Lui* [1991] proposed that the tailward-propagating rarefaction wave, generated by the pressure reduction associated with the current disruption/dipolarization, causes the plasma sheet thinning and the B_z weakening, or more taillike magnetic fields, leading to the magnetic reconnection in the midtail. At present, however, there seems to be no solid evidence to support this scenario. For discussion about the possibility, it is very important to clarify the duration of the rarefaction wave and the necessary growth time of an instability resulting in the magnetic reconnection. The thin plasma/current sheet and a very small B_z for some duration are required for efficient triggering of the magnetic reconnection.

[39] If one process causes the other, as the above scenarios, the signal of fast flow or wave should have a speed of more than 300 to 700 km/s (600 to 1400 km/s) to propagate between $-16 > X > -20\ R_E$ and $-7 > X > -10\ R_E$ within 2 (1) min. This speed is rather high. *Machida et al.* [2009] proposed a somewhat different scenario called a "catapult (slingshot) current sheet relaxation model": Magnetic field lines are highly taillike between the regions of the magnetic reconnection and the initial dipolarization. When the cross-tail current in the current sheet of this midway region is strengthened by the enhancement of the Poynting flux toward the magnetic equator, magnetic flux tubes slip earthward due to the domination of the earthward $\mathbf{J} \times \mathbf{B}$ force over the tailward pressure gradient force. The earthward flow generated by this process triggers the current disruption/dipolarization in the near-Earth region. At the same time, the earthward convection of the catapult current sheet produces

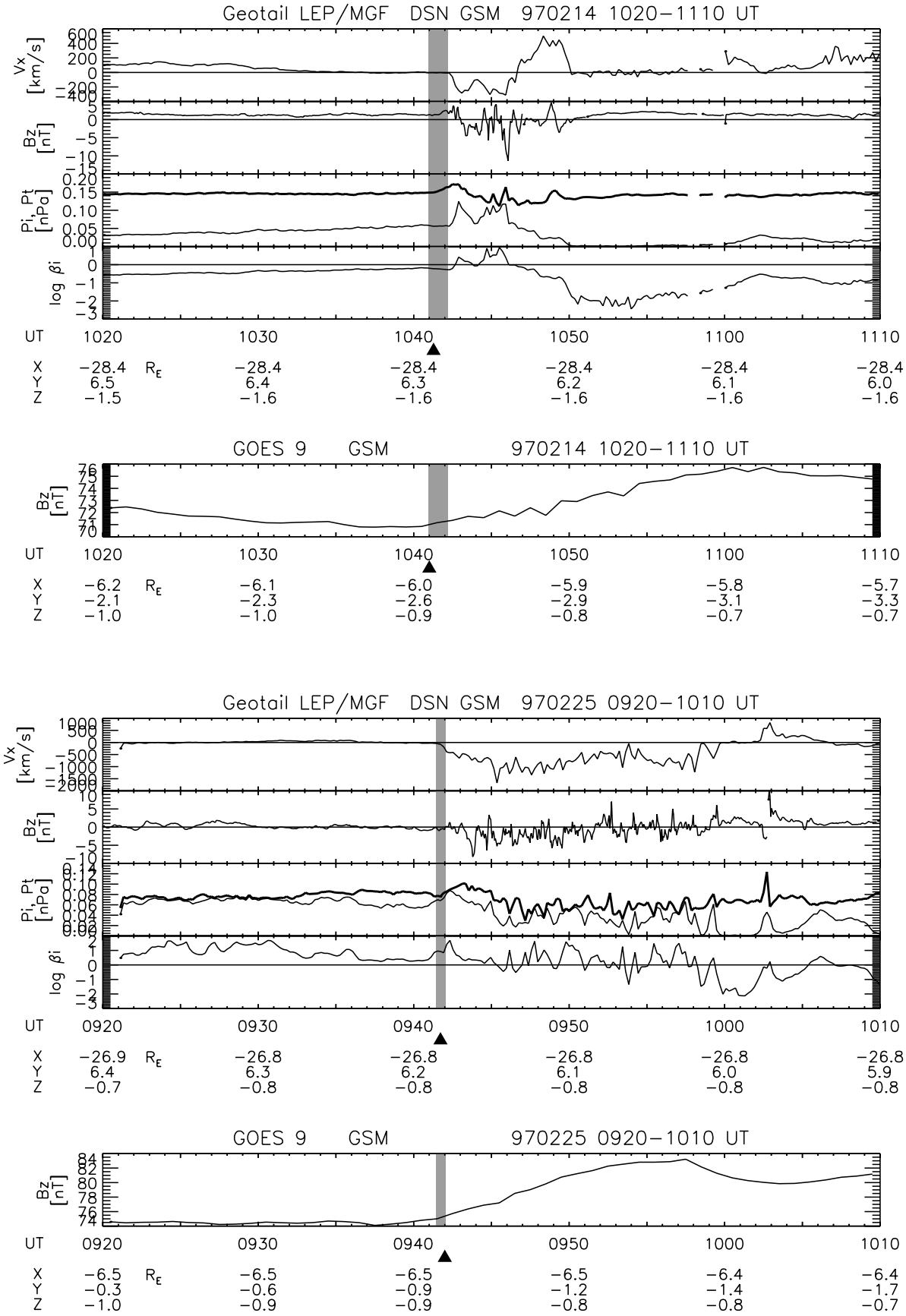
Geotail LEP/MGF DSN GSM 970214 1020–1110 UT
Vx [km/s]
Bz [nT]
Pi, Pt [nPa]
log βi
UT 1020 1030 1040 1050 1100 1110
X −28.4 R_E −28.4 −28.4 −28.4 −28.4 −28.4
Y 6.5 6.4 6.3 6.2 6.1 6.0
Z −1.5 −1.6 −1.6 −1.6 −1.6 −1.6
GOES 9 GSM 970214 1020–1110 UT
Bz [nT]
UT 1020 1030 1040 1050 1100 1110
X −6.2 R_E −6.1 −6.0 −5.9 −5.8 −5.7
Y −2.1 −2.3 −2.6 −2.9 −3.1 −3.3
Z −1.0 −1.0 −0.9 −0.8 −0.7 −0.7
Geotail LEP/MGF DSN GSM 970225 0920–1010 UT
Vx [km/s]
Bz [nT]
Pi, Pt [nPa]
log βi
UT 0920 0930 0940 0950 1000 1010
X −26.9 R_E −26.8 −26.8 −26.8 −26.8 −26.8
Y 6.4 6.3 6.2 6.1 6.0 5.9
Z −0.7 −0.8 −0.8 −0.8 −0.8 −0.8
GOES 9 GSM 970225 0920–1010 UT
Bz [nT]
UT 0920 0930 0940 0950 1000 1010
X −6.5 R_E −6.5 −6.5 −6.5 −6.4 −6.4
Y −0.3 −0.6 −0.9 −1.2 −1.4 −1.7
Z −1.0 −0.9 −0.9 −0.8 −0.8 −0.7

Figure 11

the thin current sheet at its tailward edge at $X \sim -20$ R_E, leading to the magnetic reconnection.

[40] We found that energy release is more significant between the regions of the magnetic reconnection and the initial dipolarization, which may be a key to the understanding of the causal relationship between the two processes and the substorm triggering mechanism. Possible explanations for the energy release are as follows: The region of the significant energy release is located near the earthward edge of a region of fast earthward flows, or probably the flow braking region. The low-frequency magnetic and electric field fluctuations are seen at $X \sim -14$ to -20 R_E around onset. Hence the fast flow is coupled with the Alfvén wave to convert the plasma energy into the wave energy, leading to acceleration and heating of electrons [*Angelopoulos et al.*, 2002]. Meanwhile, the total pressure enhances in the initial dipolarization region. While a large portion of the energy for this near-Earth process can be transported by the Poynting flux from the lobe [*Miyashita et al.*, 2001], some portion may be transported from the region of the significant energy release. It is an open question, however, whether the carrier is the plasma flow or some types of wave, i.e., how the energy is released, transported, and spent.

[41] The low-frequency magnetic and electric field fluctuations as well as the dawn-to-dusk electric field become large around onset at $X \sim -14$ to -20 R_E and $X \sim -10$ R_E, probably associated with the magnetic reconnection and the dipolarization, respectively. What types of wave and instability are related to these fluctuations should be investigated for the understanding of triggering mechanisms and physics of the two processes.

[42] It is likely that the magnetic reconnection is a necessary condition for the development of initial actions into a large-scale substorm [see also *Ieda et al.*, 2008], but not a sufficient condition. Plasmoids with fast tailward flows can be observed even during pseudosubstorms [e.g., *Aikio et al.*, 1999; *Ieda et al.*, 2001; *Ohtani et al.*, 2002]. Pseudosubstorms are quite similar to substorms, probably caused by the same physical process, but are generally weaker, more localized, and more short-lived than substorms, without subsequent large-scale development. Even if the magnetic reconnection proceeds to open magnetic field lines of the lobes, auroral activity does not necessarily develop significantly [*Ieda et al.*, 2001; *Ohtani et al.*, 2002]. Fast earthward flows are also observed during pseudosubstorms [e.g., *Nakamura et al.*, 2001; *Ohtani et al.*, 2002]. It is possible that their development is suppressed by some mechanism, or magnetospheric or ionospheric conditions are not favorable for full-scale development [*Kamide*, 2005]. *Ohtani et al.* [1999] suggested that the current disruption or dipolarization can play a crucial role in the development of substorms. Ionospheric conditions may also be important for the substorm development. Further detailed studies are needed for understanding magnetospheric and ionospheric conditions for the onset and development of substorms as well as the causality of the magnetic reconnection and the current disruption.

[43] The present analyses showed that the magnetic reconnection site, or the "near-Earth neutral line", at substorm expansion onset is located at $X \sim -16$ to -20 R_E on average. The location in individual cases, however, varies depending on the substorm intensity: it tends to be located closer to the Earth in more intense substorms [*Miyashita et al.*, 2004]. In rare cases, the magnetic reconnection can occur at $X \sim -13$ R_E [*Baker et al.*, 1996], and even earthward of $X \sim -8$ R_E or $R \sim 12$ R_E [*Miyashita et al.*, 2005b] and $R \sim 9$ R_E [*Miyashita et al.*, 2005a].

[44] From the viewpoint of the magnetotail structure, the magnetic reconnection appears to occur near the tailward edge of the thin current sheet or the transition from dipolelike to taillike field, which may extend from the near-Earth region to $X \sim -20$ R_E. A region of considerably taillike magnetic field lines extends from $X \sim -5$ to -20 R_E, as shown in Figure 2 (middle). The radial gradient of B_z becomes very small at $X \sim -15$ to -18 R_E [*Miyashita et al.*, 2003]. *Miyashita et al.* [2004] also showed the same results for intense and weak substorms. These results are consistent with those of *Asano et al.* [2004], who proposed that the magnetic reconnection occurs near the tailward edge of the thin current sheet. Here, for understanding of the substorm triggering, we think it very important to consider the differences in the current sheet structure as well as the characteristics of plasma flows, such as width, between the earthward and tailward sides of the magnetic reconnection region, as *Miyashita et al.* [2003] also discussed.

[45] It is extremely important to understand what controls the triggering and location of the near-Earth magnetic reconnection. Magnetic field lines become more taillike during energy accumulation in the magnetotail in the substorm growth phase, resulting in favorable configuration for the magnetic reconnection and earthward movement of the transition region. However, some substorms seem to occur even in the course of energy accumulation, while some other substorms do not seem to be triggered effectively in spite of continuous energy accumulation. It is possible that conditions other than the amount of stored energy in the magnetotail are necessary for the substorm initiation. For

Figure 11. From top to bottom are the GSM X component of the ion flow V_x, the north-south magnetic field B_z, the total (top line, P_t) and ion (bottom line, P_i) pressures, and the ion β from Geotail, and B_z from GOES 9 for two substorm events that occurred (top event) at 1041:35 UT ±37 s on 14 February 1997 and (bottom event) at 0941:44 UT ±18 s on 25 February 1997. The substorm onset times were determined from the Polar UVI data and indicated by the vertical lines. The initial auroral brightenings occurred at ~67° AACGM latitude and ~23 hr MLT for both substorms. For the 25 February 1997 event, a pseudobreakup occurred at ~68° latitude and ~0 hr MLT at 0934:59 UT ±18 s before the substorm onset. The time resolutions of the ion moments from Geotail LEP, B_z from Geotail MGF, and B_z from GOES 9 are 12 s, 3 s, and 1 min, respectively. The ion pressure shown was calculated only from the LEP data. The solid triangles at the bottom indicate the times when Geotail and GOES 9 began to observe the plasmoid in the midtail and the dipolarization in the near-Earth tail, respectively, associated with the substorm onsets. The start of the plasmoid is identified by the total pressure enhancement [cf. *Ieda et al.*, 1998].

example, the interaction between the distant and near-Earth reconnection sites may be important [*Russell*, 2000]. *Nagai et al.* [2005] proposed that the near-Earth magnetic reconnection site is controlled by the solar wind electric field or the efficiency of the solar wind energy input. Further studies are necessary for the role of external and internal conditions for the substorm triggering.

[46] The difference between the first and following onsets of multiple substorm events is an interesting issue. In the present study we did not distinguish between the first and following onsets, that is, we selected not only the first onset but also the second and third (if any) onsets in the case of a multiple onset event. In contrast, *Machida et al.* [1999] and *Miyashita et al.* [1999, 2000] selected only the first onsets. The auroral breakups from IMAGE FUV used in the present study are also the first onsets; using only them, we have performed the superposed epoch analysis. From these analyses, we obtained almost the same statistical features that obtained in the present study. In fact, both plasmoid and dipolarization occur for each onset of multiple events [e.g., *Ieda et al.*, 2001; *Slavin et al.*, 2002]. We infer from these results that magnetotail variations phenomenologically do not differ between the first and following onsets. It is, however, important to examine in detail the quantitative difference, since the precondition, i.e., whether or not the effect of the previous substorm still remains, is different. It is also interesting to compare multiple substorms with isolated substorms.

[47] In conclusion, as discussed above, the causal relationship between the magnetic reconnection and the dipolarization as well as detailed mechanisms of each of the two processes still remains a crucial issue concerning the substorm triggering. However, the present statistical results provide a state-of-the-art framework of magnetotail evolution associated with substorm expansion onset. The framework will be helpful as a reference guide to developing the overall picture of magnetotail evolution and studying the detailed mechanisms of the substorm triggering on the basis of multispacecraft observations with a higher time resolution, such as the THEMIS mission.

[48] **Acknowledgments.** The Geotail MGF magnetic field data were provided by S. Kokubun and T. Nagai. The Geotail EPIC high-energy particle data were provided by R.W. McEntire and A.T.Y. Lui. We thank Y. Ono for preparing the EPIC data. The GOES magnetic field data were provided by H.J. Singer through the Coordinated Data Analysis Web (CDAWeb) at NASA. The Polar UVI and IMAGE FUV auroral imager data were provided by G.K. Parks and S.B. Mende, respectively. We thank Y. Asano for his useful comments.

[49] Zuyin Pu thanks Victor Sergeev and another reviewer for their assistance in evaluating this paper.

References

Aikio, A. T., V. A. Sergeev, M. A. Shukhtina, L. I. Vagina, V. Angelopoulos, and G. D. Reeves (1999), Characteristics of pseudobreakups and substorms observed in the ionosphere, at the geosynchronous orbit, and in the midtail, *J. Geophys. Res.*, *104*(A6), 12,263–12,287.

Angelopoulos, V., C. F. Kennel, F. V. Coroniti, R. Pellat, M. G. Kivelson, R. J. Walker, C. T. Russell, W. Baumjohann, W. C. Feldman, and J. T. Gosling (1994), Statistical characteristics of bursty bulk flow events, *J. Geophys. Res.*, *99*(A11), 21,257–21,280.

Angelopoulos, V., et al. (1997), Magnetotail flow bursts: Association to global magnetospheric circulation, relationship to ionospheric activity and direct evidence for localization, *Geophys. Res. Lett.*, *24*(18), 2271–2274.

Angelopoulos, V., J. A. Chapman, F. S. Mozer, J. D. Scudder, C. T. Russell, K. Tsuruda, T. Mukai, T. J. Hughes, and K. Yumoto (2002), Plasma sheet electromagnetic power generation and its dissipation along auroral field lines, *J. Geophys. Res.*, *107*(A8), 1181, doi:10.1029/2001JA900136.

Angelopoulos, V., et al. (2008), Tail reconnection triggering substorm onset, *Science*, *321*(5891), 931–935.

Asano, Y., T. Mukai, M. Hoshino, Y. Saito, H. Hayakawa, and T. Nagai (2004), Statistical study of thin current sheet evolution around substorm onset, *J. Geophys. Res.*, *109*, A05213, doi:10.1029/2004JA010413.

Baker, D. N., T. I. Pulkkinen, V. Angelopoulos, W. Baumjohann, and R. L. McPherron (1996), Neutral line model of substorms: Past results and present view, *J. Geophys. Res.*, *101*(A6), 12,975–13,010.

Baumjohann, W., G. Paschmann, and C. A. Cattell (1989), Average plasma properties in the central plasma sheet, *J. Geophys. Res.*, *94*(A6), 6597–6606.

Baumjohann, W., M. Hesse, S. Kokubun, T. Mukai, T. Nagai, and A. A. Petrukovich (1999), Substorm dipolarization and recovery, *J. Geophys. Res.*, *104*(A11), 24,995–25,000.

Bhattacharjee, A., Z. W. Ma, and X. Wang (1998), Ballooning instability of a thin current sheet in the high-Lundquist-number magnetotail, *Geophys. Res. Lett.*, *25*(6), 861–864.

Cao, X., et al. (2008), Multispacecraft and ground-based observations of substorm timing and activations: Two case studies, *J. Geophys. Res.*, *113*, A07S25, doi:10.1029/2007JA012761.

Cheng, C. Z., and A. T. Y. Lui (1998), Kinetic ballooning instability for substorm onset and current disruption observed by AMPTE/CCE, *Geophys. Res. Lett.*, *25*(21), 4091–4094.

Frey, H. U., and S. B. Mende (2007), Substorm onsets as observed by IMAGE-FUV, in *Proceedings of International Conference on Substorms-8*, edited by M. Syrjäsuo and E. Donovan, pp. 71–75, Univ. of Calgary, Alta., Canada.

Frey, H. U., S. B. Mende, V. Angelopoulos, and E. F. Donovan (2004), Substorm onset observations by IMAGE-FUV, *J. Geophys. Res.*, *109*, A10304, doi:10.1029/2004JA010607.

Goertz, C. K., and R. A. Smith (1989), The thermal catastrophe model of substorms, *J. Geophys. Res.*, *94*(A6), 6581–6596.

Hones, E. W., Jr. (1976), The magnetotail: Its generation and dissipation, in *Physics of Solar Planetary Environments*, edited by D. J. Williams, pp. 558–571, AGU, Washington, D. C.

Ieda, A., S. Machida, T. Mukai, Y. Saito, T. Yamamoto, A. Nishida, T. Terasawa, and S. Kokubun (1998), Statistical analysis of the plasmoid evolution with Geotail observations, *J. Geophys. Res.*, *103*(A3), 4453–4465.

Ieda, A., D. H. Fairfield, T. Mukai, Y. Saito, S. Kokubun, K. Liou, C.-I. Meng, G. K. Parks, and M. J. Brittnacher (2001), Plasmoid ejection and auroral brightenings, *J. Geophys. Res.*, *106*(A3), 3845–3857.

Ieda, A., et al. (2008), Longitudinal association between magnetotail reconnection and auroral breakup based on Geotail and Polar observations, *J. Geophys. Res.*, *113*, A08207, doi:10.1029/2008JA013127.

Jacquey, C., J. A. Sauvaud, and J. Dandouras (1991), Location and propagation of the magnetotail current disruption during substorm expansion: Analysis and simulation of an ISEE multi-onset event, *Geophys. Res. Lett.*, *18*(3), 389–392.

Kamide, Y. (2005), What determines the intensity of magnetospheric substorms?, in *Multiscale Coupling of Sun-Earth Processes*, edited by A. T. Y. Lui, Y. Kamide, and G. Consolini, pp. 175–194, Elsevier, New York.

Kan, J. R. (2007), On the formation of near-Earth X-line at substorm expansion onset, *J. Geophys. Res.*, *112*, A01207, doi:10.1029/2006JA012011.

Kan, J. R., L. Zhu, and S.-I. Akasofu (1988), A theory of substorms: Onset and subsidence, *J. Geophys. Res.*, *93*(A6), 5624–5640.

Kistler, L. M., E. Möbius, W. Baumjohann, G. Paschmann, and D. C. Hamilton (1992), Pressure changes in the plasma sheet during substorm injections, *J. Geophys. Res.*, *97*(A3), 2973–2983.

Kokubun, S., T. Yamamoto, M. H. Acuña, K. Hayashi, K. Shiokawa, and H. Kawano (1994), The GEOTAIL magnetic field experiment, *J. Geomagn. Geoelectr.*, *46*(1), 7–21.

Liou, K., C.-I. Meng, P. T. Newell, K. Takahashi, S.-I. Ohtani, A. T. Y. Lui, M. Brittnacher, and G. Parks (2000), Evaluation of low-latitude Pi2 pulsations as indicators of substorm onset using Polar ultraviolet imagery, *J. Geophys. Res.*, *105*(A2), 2495–2505.

Liou, K., C.-I. Meng, A. T. Y. Lui, P. T. Newell, and S. Wing (2002), Magnetic dipolarization with substorm expansion onset, *J. Geophys. Res.*, *107*(A7), 1131, doi:10.1029/2001JA000179.

Lui, A. T. Y. (1991), A synthesis of magnetospheric substorm models, *J. Geophys. Res.*, *96*(A2), 1849–1856.

Lui, A. T. Y. (1996), Current disruption in the Earth's magnetosphere: Observations and models, *J. Geophys. Res.*, *101*(A6), 13,067–13,088.

Lui, A. T. Y., C.-L. Chang, A. Mankofsky, H.-K. Wong, and D. Winske (1991), A cross-field current instability for substorm expansions, *J. Geophys. Res.*, *96*(A7), 11,389–11,401.

Lui, A. T. Y., R. E. Lopez, B. J. Anderson, K. Takahashi, L. J. Zanetti, R. W. McEntire, T. A. Potemra, D. M. Klumpar, E. M. Greene, and R. Strangeway

(1992), Current disruptions in the near-Earth neutral sheet region, *J. Geophys. Res.*, *97*(A2), 1461–1480.
Lui, A. T. Y., K. Liou, P. T. Newell, C.-I. Meng, S.-I. Ohtani, T. Ogino, S. Kokubun, M. J. Brittnacher, and G. K. Parks (1998), Plasma and magnetic flux transport associated with auroral breakups, *Geophys. Res. Lett.*, *25*(21), 4059–4062.
Lui, A. T. Y., K. Liou, M. Nosé, S. Ohtani, D. J. Williams, T. Mukai, K. Tsuruda, and S. Kokubun (1999), Near-Earth dipolarization: Evidence for a non-MHD process, *Geophys. Res. Lett.*, *26*(19), 2905–2908.
Lui, A. T. Y., Y. Zheng, H. Rème, M. W. Dunlop, G. Gustafsson, and C. J. Owen (2007), Breakdown of the frozen-in condition in the Earth's magnetotail, *J. Geophys. Res.*, *112*, A04215, doi:10.1029/2006JA012000.
Lyons, L. R. (1995), A new theory for magnetospheric substorms, *J. Geophys. Res.*, *100*(A10), 19,069–19,081.
Lyons, L. R., C.-P. Wang, T. Nagai, T. Mukai, Y. Saito, and J. C. Samson (2003), Substorm inner plasma sheet particle reduction, *J. Geophys. Res.*, *108*(A12), 1426, doi:10.1029/2003JA010177.
Machida, S., Y. Miyashita, A. Ieda, A. Nishida, T. Mukai, Y. Saito, and S. Kokubun (1999), GEOTAIL observations of flow velocity and north-south magnetic field variations in the near and mid-distant tail associated with substorm onsets, *Geophys. Res. Lett.*, *26*(6), 635–638.
Machida, S., Y. Miyashita, A. Ieda, M. Nosé, D. Nagata, K. Liou, T. Obara, A. Nishida, Y. Saito, and T. Mukai (2009), Statistical visualization of the Earth's magnetotail based on Geotail data and the implied substorm model, *Ann. Geophys.*, in press.
Mende, S. B., et al. (2000a), Far ultraviolet imaging from the IMAGE spacecraft. 1: System design, *Space Sci. Rev.*, *91*(1–2), 243–270.
Mende, S. B., et al. (2000b), Far ultraviolet imaging from the IMAGE spacecraft. 2: Wideband FUV imaging, *Space Sci. Rev.*, *91*(1–2), 271–285.
Mende, S. B., et al. (2000c), Far ultraviolet imaging from the IMAGE spacecraft. 3: Spectral imaging of Lyman-α and OI 135.6 nm, *Space Sci. Rev.*, *91*(1–2), 287–318.
Miyashita, Y., S. Machida, A. Nishida, T. Mukai, Y. Saito, and S. Kokubun (1999), GEOTAIL observations of total pressure and electric field variations in the near and mid-distant tail associated with substorm onsets, *Geophys. Res. Lett.*, *26*(6), 639–642.
Miyashita, Y., S. Machida, T. Mukai, Y. Saito, K. Tsuruda, H. Hayakawa, and P. R. Sutcliffe (2000), A statistical study of variations in the near and middistant magnetotail associated with substorm onsets: GEOTAIL observations, *J. Geophys. Res.*, *105*(A7), 15,913–15,930.
Miyashita, Y., S. Machida, T. Mukai, Y. Saito, and P. R. Sutcliffe (2001), Mass and energy transport in the near and middistant magnetotail around substorm onsets: Geotail observations, *J. Geophys. Res.*, *106*(A4), 6259–6274.
Miyashita, Y., S. Machida, K. Liou, T. Mukai, Y. Saito, H. Hayakawa, C.-I. Meng, and G. K. Parks (2003), Evolution of the magnetotail associated with substorm auroral breakups, *J. Geophys. Res.*, *108*(A9), 1353, doi:10.1029/2003JA009939.
Miyashita, Y., Y. Kamide, S. Machida, K. Liou, T. Mukai, Y. Saito, A. Ieda, C.-I. Meng, and G. K. Parks (2004), Difference in magnetotail variations between intense and weak substorms, *J. Geophys. Res.*, *109*, A11205, doi:10.1029/2004JA010588.
Miyashita, Y., et al. (2005a), Geotail observations of signatures in the near-Earth magnetotail for the extremely intense substorms of the 30 October 2003 storm, *J. Geophys. Res.*, *110*, A09S25, doi:10.1029/2005JA011070.
Miyashita, Y., et al. (2005b), Plasmoids observed in the near-Earth magnetotail at $X \sim 7\ R_E$, *J. Geophys. Res.*, *110*, A12214, doi:10.1029/2005JA011263.
Mukai, T., S. Machida, Y. Saito, M. Hirahara, T. Terasawa, N. Kaya, T. Obara, M. Ejiri, and A. Nishida (1994), The low energy particle (LEP) experiment onboard the GEOTAIL satellite, *J. Geomagn. Geoelectr.*, *46*(8), 669–692.
Nagai, T. (1982), Observed magnetic substorm signatures at synchronous altitude, *J. Geophys. Res.*, *87*(A6), 4405–4417.
Nagai, T., M. Fujimoto, Y. Saito, S. Machida, T. Terasawa, R. Nakamura, T. Yamamoto, T. Mukai, A. Nishida, and S. Kokubun (1998), Structure and dynamics of magnetic reconnection for substorm onsets with Geotail observations, *J. Geophys. Res.*, *103*(A3), 4419–4440.
Nagai, T., M. Fujimoto, R. Nakamura, W. Baumjohann, A. Ieda, I. Shinohara, S. Machida, Y. Saito, and T. Mukai (2005), Solar wind control of the radial distance of the magnetic reconnection site in the magnetotail, *J. Geophys. Res.*, *110*, A09208, doi:10.1029/2005JA011207.
Nakamura, R., W. Baumjohann, M. Brittnacher, V. A. Sergeev, M. Kubyshkina, T. Mukai, and K. Liou (2001), Flow bursts and auroral activations: Onset timing and foot point location, *J. Geophys. Res.*, *106*(A6), 10,777–10,789.
Nakamura, R., et al. (2004), Spatial scale of high-speed flows in the plasma sheet observed by Cluster, *Geophys. Res. Lett.*, *31*, L09804, doi:10.1029/2004GL019558.
Ohtani, S. (1998), Earthward expansion of tail current disruption: Dual-satellite study, *J. Geophys. Res.*, *103*(A4), 6815–6825.
Ohtani, S., S. Kokubun, and C. T. Russell (1992), Radial expansion of the tail current disruption during substorms: A new approach to the substorm onset region, *J. Geophys. Res.*, *97*(A3), 3129–3136.
Ohtani, S., F. Creutzberg, T. Mukai, H. Singer, A. T. Y. Lui, M. Nakamura, P. Prikryl, K. Yumoto, and G. Rostoker (1999), Substorm onset timing: The December 31, 1995, event, *J. Geophys. Res.*, *104*(A10), 22,713–22,727.
Ohtani, S., R. Yamaguchi, M. Nosé, H. Kawano, M. Engebretson, and K. Yumoto (2002), Quiet time magnetotail dynamics and their implications for the substorm trigger, *J. Geophys. Res.*, *107*(A2), 1030, doi:10.1029/2001JA000116.
Ohtani, S., H. J. Singer, and T. Mukai (2006), Effects of the fast plasma sheet flow on the geosynchronous magnetic configuration: Geotail and GOES coordinated study, *J. Geophys. Res.*, *111*, A01204, doi:10.1029/2005JA011383.
Petrukovich, A. A., et al. (1998), Two spacecraft observations of a reconnection pulse during an auroral breakup, *J. Geophys. Res.*, *103*(A1), 47–59.
Pu, Z. Y., et al. (1999), Ballooning instability in the presence of a plasma flow: A synthesis of tail reconnection and current disruption models for the initiation of substorms, *J. Geophys. Res.*, *104*(A5), 10,235–10,248.
Pu, Z. Y., A. Korth, Z. X. Chen, Z. X. Liu, S. Y. Fu, G. Zong, M. H. Hong, and X. M. Wang (2001), A global synthesis model of dipolarization at substorm expansion onset, *J. Atmos. Sol. Terr. Phys.*, *63*(7), 671–681.
Pulkkinen, T. I., and M. Wiltberger (2000), Thin current sheet evolution as seen in observations, empirical models and MHD simulations, *Geophys. Res. Lett.*, *27*(9), 1363–1366.
Pulkkinen, T. I., D. N. Baker, L. L. Cogger, L. A. Frank, J. B. Sigwarth, S. Kokubun, T. Mukai, H. J. Singer, J. A. Slavin, and L. Zelenyi (1999), Spatial extent and dynamics of a thin current sheet during the substorm growth phase on December 10, 1996, *J. Geophys. Res.*, *104*(A12), 28,475–28,490.
Rostoker, G. (1996), Phenomenology and physics of magnetospheric substorms, *J. Geophys. Res.*, *101*(A6), 12,955–12,973.
Rostoker, G., and T. Eastman (1987), A boundary layer model for magnetospheric substorms, *J. Geophys. Res.*, *92*(A11), 12,187–12,201.
Rothwell, P. L., L. P. Block, M. B. Silevitch, and C.-G. Fälthammar (1988), A new model for substorm onsets: The pre-breakup and triggering regimes, *Geophys. Res. Lett.*, *15*(11), 1279–1282.
Roux, A., S. Perraut, P. Robert, A. Morane, A. Pedersen, A. Korth, G. Kremser, B. Aparicio, D. Rodgers, and R. Pellinen (1991), Plasma sheet instability related to the westward traveling surge, *J. Geophys. Res.*, *96*(A10), 17,697–17,714.
Runov, A., et al. (2003), Current sheet structure near magnetic X-line observed by Cluster, *Geophys. Res. Lett.*, *30*(11), 1579, doi:10.1029/2002GL016730.
Russell, C. T. (1972), The configuration of the magnetosphere, in *Critical Problems of Magnetospheric Physics*, edited by E. R. Dyer, pp. 1–16, IUCSTP Secr., Washington, D. C.
Russell, C. T. (1974), The solar wind and magnetospheric dynamics, in *Correlated Interplanetary and Magnetospheric Observations*, edited by D. E. Page, pp. 3–47, Springer, New York.
Russell, C. T. (2000), How northward turnings of the IMF can lead to substorm expansion onsets, *Geophys. Res. Lett.*, *27*(20), 3257–3259.
Russell, C. T., R. C. Snare, J. D. Means, D. Pierce, D. Dearborn, M. Larson, G. Barr, and G. Le (1995), The GGS/Polar magnetic fields investigation, *Space Sci. Rev.*, *71*(1–4), 563–582.
Saito, M. H., Y. Miyashita, M. Fujimoto, I. Shinohara, Y. Saito, K. Liou, and T. Mukai (2008), Ballooning mode waves prior to substorm-associated dipolarizations: Geotail observations, *Geophys. Res. Lett.*, *35*, L07103, doi:10.1029/2008GL033269.
Samson, J. C., L. R. Lyons, P. T. Newell, F. Creutzberg, and B. Xu (1992), Proton aurora and substorm intensifications, *Geophys. Res. Lett.*, *19*(21), 2167–2170.
Schödel, R., W. Baumjohann, R. Nakamura, V. A. Sergeev, and T. Mukai (2001), Rapid flux transport in the central plasma sheet, *J. Geophys. Res.*, *106*(A1), 301–313.
Shiokawa, K., W. Baumjohann, and G. Haerendel (1997), Braking of high-speed flows in the near-Earth tail, *Geophys. Res. Lett.*, *24*(10), 1179–1182.
Shiokawa, K., et al. (1998), High-speed ion flow, substorm current wedge, and multiple Pi 2 pulsations, *J. Geophys. Res.*, *103*(A3), 4491–4507.
Slavin, J. A., et al. (1999), Dual spacecraft observations of lobe magnetic field perturbations before, during and after plasmoid release, *Geophys. Res. Lett.*, *26*(19), 2897–2900.
Slavin, J. A., et al. (2002), Simultaneous observations of earthward flow bursts and plasmoid ejection during magnetospheric substorms, *J. Geophys. Res.*, *107*(A7), 1106, doi:10.1029/2000JA003501.
Smith, R. A., C. K. Goertz, and W. Grossmann (1986), Thermal catastrophe in the plasma sheet boundary layer, *Geophys. Res. Lett.*, *13*(13), 1380–1383.

Taguchi, S., M. Kiyohara, T. Mukai, T. Yamamoto, M. Nose, Y. Saito, and S. Kokubun (1998), Geotail observations of north-south plasma velocity enhancements in the lobe near substorm expansion phase onset, *Geophys. Res. Lett.*, *25*(22), 4125–4128.

Takada, T., R. Nakamura, W. Baumjohann, Y. Asano, M. Volwerk, T. L. Zhang, B. Klecker, H. Rème, E. A. Lucek, and C. Carr (2006), Do BBFs contribute to inner magnetosphere dipolarizations: Concurrent Cluster and Double Star observations, *Geophys. Res. Lett.*, *33*, L21109, doi:10.1029/2006GL027440.

Torr, M. R., et al. (1995), A far ultraviolet imager for the international solar-terrestrial physics mission, *Space Sci. Rev.*, *71*(1–4), 329–383.

Tsuruda, K., H. Hayakawa, M. Nakamura, T. Okada, A. Matsuoka, F. S. Mozer, and R. Schmidt (1994), Electric field measurements on the GEOTAIL satellite, *J. Geomagn. Geoelectr.*, *46*(8), 693–711.

Williams, D. J., R. W. McEntire, C. Schlemm II, A. T. Y. Lui, G. Gloeckler, S. P. Christon, and F. Gliem (1994), GEOTAIL energetic particles and ion composition instrument, *J. Geomagn. Geoelectr.*, *46*(1), 39–57.

Zhang, H., et al. (2007), TC-1 observations of flux pileup and dipolarization-associated expansion in the near-Earth magnetotail during substorms, *Geophys. Res. Lett.*, *34*, L03104, doi:10.1029/2006GL028326.

S. P. Christon, Focused Analysis and Research, 11043 Berrypick Lane, Columbia, MD 21044, USA.

H. U. Frey, Space Sciences Laboratory, University of California, 7 Gauss Way, Berkeley, CA 94720, USA.

M. Fujimoto, H. Hayakawa, Y. Miyashita, T. Mukai, M. H. Saito, Y. Saito, and I. Shinohara, Institute of Space and Astronautical Science, Japan Aerospace Exploration Agency, 3-1-1 Yoshinodai, Sagamihara, Kanagawa 229-8510, Japan. (miyasita@stp.isas.jaxa.jp)

A. Ieda, Solar-Terrestrial Environment Laboratory, Nagoya University, Furo-cho, Chikusa-ku, Nagoya, Aichi 464-8601, Japan.

Y. Kamide, Research Institute for Sustainable Humanosphere, Kyoto University, Gokasho, Uji, Kyoto 611-0011, Japan.

K. Liou, Applied Physics Laboratory, Johns Hopkins University, 11100 Johns Hopkins Road, Laurel, MD 20723, USA.

S. Machida and D. Nagata, Department of Geophysics, Kyoto University, Kitashirakawa-Oiwake-cho, Sakyo-ku, Kyoto 606-8502, Japan.

M. Nosé, Data Analysis Center for Geomagnetism and Space Magnetism, Graduate School of Science, Kyoto University, Kitashirakawa-Oiwake-cho, Sakyo-ku, Kyoto 606-8502, Japan.

C. T. Russell, Institute of Geophysics and Planetary Physics, University of California, 6843 Slichter Hall, Los Angeles, CA 90024-1567, USA.